Running head:

Ancient tidally modulated shoreface deposits

Title:

Characteristics and context of high-energy, tidally modulated, barred shoreface deposits: Kimmeridgian–Tithonian sandstones, Weald Basin, southern UK and northern France

Authors:

LYNSEY ANGUS[1], GARY J. HAMPSON*, FRANCESCO PALCI[2], ALASTAIR J. FRASER

Department of Earth Science and Engineering, Imperial College London, South Kensington Campus, London SW7 2AZ, UK.

[1]present address: Total S.A., Avenue Larribau, Pau, France.

[2]present address: UK Oil & Gas plc., Broadgate Tower, 20 Primrose Street, London EC2A 2EW, UK.

*Corresponding author e-mail: g.j.hampson@imperial.ac.uk

Key words:

tidally modulated shoreface, Kimmeridgian, Tithonian, Weald Basin

Word count (abstract):	388
Word count (text):	9579
Word count (references):	3331
Word count (figure captions):	1825
Number of figures:	15
Number of tables:	0

ABSTRACT

The influence of tides on the sedimentology of wave-dominated shorefaces has been emphasized in recent studies of modern shorelines and related facies models, but few ancient examples have been reported to date. Herein, we use a case study from the stratigraphic record to develop a revised facies model and predictive spatio-temporal framework for high-energy, tidally modulated, wave-dominated, barred shorefaces.

Kimmeridgian–Tithonian shallow-marine sandstones in the Weald Basin (southern England and northern France) occur as a series of laterally extensive tongues that are 5–24 m thick. Each tongue coarsens upward in its lower part and fines upward in its upper part. The lower part of each upward-coarsening succession consists of variably stacked, hummocky cross-stratified, very fine- to fine-grained sandstone beds and mudstone interbeds that are moderately to intensely bioturbated by a mixed *Skolithos* and *Cruziana* ichnofacies. This lower part of the succession is interpreted to record deposition on the subtidal lower shoreface, between effective storm wave base and fairweather wave base. The upper part of each upward-coarsening succession comprises cross-bedded, medium- to coarse-grained sandstones that are pervasively intercalated with mudstone-draped, wave-rippled surfaces (including interference ripples) which mantle the erosional bases of trough cross-sets. Bioturbation is patchy, and constitutes a low-diversity *Skolithos* ichnofacies. Cross-bedded sandstones are arranged into cosets superimposed on steeply dipping (up to 10˚) clinoforms that dip offshore and alongshore, and extend through the succession. These deposits are interpreted to record shallow subtidal and intertidal bars on the upper shoreface, which likely contained laterally migrating rip channels or formed part of a spit. The lower, upward-coarsening part of each sandstone tongue represents an upward-shallowing, regressive shoreface succession in which the internal bedding of upper-shoreface sandstones was modulated by tidal changes in water depth. The upper, upward-fining part of each sandstone tongue typically comprises an erosionally based bioclastic lag overlain by subtidal lower-shoreface deposits, and constitutes an upward-deepening succession developed during transgression.

Regressive–transgressive sandstone tongues fringe the northeastern margin of the basin, which was exposed to an energetic wave climate driven by westerly and southwesterly winds with a fetch of 200–600 km. The high tidal range interpreted from the shoreface sandstone tongues is attributed to resonant amplification in a broad (150–200 km), shallow (18–33 m) embayment as the tidal wave propagated from the Tethys Ocean into the adjacent intracratonic Laurasian Seaway, of which the Weald Basin was a part.

[end of abstract]

INTRODUCTION

Mixed-process regimes, which are characterized by the interaction of wave, tidal, and/or fluvial processes, are emphasized in recently developed interpretive frameworks for shallow-marine strata (e.g., Yoshida et al. 2007; Ainsworth et al. 2008, 2011; Rossi et al. 2017). However, the facies models associated with these mixed-process frameworks have been based on a small number of case studies to date. Furthermore, the predictions arising from these frameworks of stratigraphic and paleogeographic context for mixed-influence shallow-marine deposits also require testing against a wider range of modern and ancient examples. This paper presents a case study that expands on recent facies models of wave-dominated shoreface sandstones in which tides had a significant effect (Dashtgard et al. 2009, 2012; Vakarelov et al. 2012). The studied shallow-marine sandstones are of Kimmeridgian–Tithonian age, and were deposited in the Weald Basin of southern England and northern France. Previous studies have documented possible tide and wave influence in these sandstones, which have been variously interpreted as storm-dominated offshore sand ridges (Sun 1992), mixed wave- and tide-dominated estuaries developed in an embayment (Proust et al. 1995), “unusual” fairweather-wave-dominated shorefaces (Wignall et al. 1996), sharp-based “lowstand” shorefaces that are locally cut into by tidal inlets (Mahieux et al. 1998; Proust et al. 2001), storm-dominated “lowstand” deposits (Taylor and Sellwood 2002), and storm-dominated shorefaces (Schlirf 2003). In contrast to these previous interpretations, we consider the interpretation of these sandstones as the deposits of tidally modulated shorefaces.

Regressive wave-dominated shoreface–shelf deposits exhibit a characteristic upward-coarsening vertical succession in which sedimentary structures record a progressive upward change from intermittent storm-wave activity to the continuous action of shoaling and then breaking fairweather waves (e.g., Clifton 1976, 2006). Each such regressive succession contains a set of seaward-dipping clinoforms (e.g., Hampson et al. 2008). Differences between regressive wave-dominated shoreface successions have generally been attributed to variability in grain size, wave energy, and shoreface morphology, related to the presence or absence of longshore bars (e.g., Figure 7.11 in Elliott 1986; Clifton 2006). The effects of tides in regressive wave-dominated shoreface successions can either be direct, in the form of structures generated by strong tidal currents (“tide-influenced shorefaces” *sensu* Dashtgard et al. 2012), or indirect, reflecting lateral migration of wave-generated facies belts along the shoreface–shelf profile in response to changing water depth during a tidal cycle (“tidally modulated shorefaces" *sensu* Dashtgard et al. 2012). The strong tidal currents and relatively weak storm-wave energy that lead to development of tide-influenced shorefaces are inferred to require bathymetric constriction of the tidal wave in a sheltered setting, such as straits (e.g., modern Juan de Fuca Strait, Canada; Frey and Dashtgard 2011; Dashtgard et al. 2012). Tidally modulated shorefaces are inferred to be developed in settings with a large tidal range (e.g., modern Waterside Beach, Bay of Fundy, Canada; Dashtgard et al. 2009, 2012 and modern Berck Plage, northern France; Vaucher et al. 2018). To date, only three ancient examples of regressive wave-dominated shoreface sandstones that were affected by tides have been documented, in the Ordovician Fezouata and Zini formations, peri-Gondwanaland shelf, Morocco (Vaucher et al. 2017), Jurassic Plover Formation, Bonaparte Basin, offshore Australia (Ainsworth et al. 2008), and the Cretaceous Bearpaw to Horseshoe Canyon Formation, Alberta Basin, Canada (Vakarelov et al. 2012). Tidal influence is more much widely interpreted in transgressive barrier-island systems that are fronted by wave-dominated shoreface–shelf deposits, although shoreface deposits are only rarely preserved in such systems (e.g., Nummedal and Swift 1987; Cattaneo and Steel 2003; Sixsmith et al. 2008).

In this paper, we document the sedimentologic character of Kimmeridgian–Tithonian sandstones in the Weald Basin of southern England and northern France, using a combination of outcrop and core data. The aims of the paper are threefold: (1) to describe the facies characteristics of these shallow-marine sandstones, which exhibit both wave and tide influence, (2) to present a model for deposition of the sandstones in a series of high-energy, tidally modulated, barred shorefaces, and (3) to evaluate the stratigraphic and paleogeographic controls on the development and distribution of these shorefaces.

GEOLOGIC SETTING

The studied shallow-marine sandstones occur in Kimmeridgian–Tithonian strata of the northeastern Weald Basin (Fig. 1). The Weald Basin is an intracratonic, extensional basin of Permian to Cretaceous age that is bounded by west–east-trending zones of normal faults (Chadwick 1986; Hansen et al. 2002; Mansy et al. 2003). The basin was inverted and uplifted during the Cenozoic, resulting in erosional exhumation of Jurassic and Cretaceous strata in its center (Chadwick 1986; Hansen et al. 2002; Mansy et al. 2003; Andrews 2014) (Fig. 2).

At the present day, strata of Kimmeridgian–Tithonian age lie in the subsurface of southern England and crop out in the Boulonnais region of northern France (Fig. 2). In southern England, these strata have mostly been assigned to the Kimmeridge Clay Formation (e.g., Andrews 2014), although strata of early Kimmeridgian age, which contain several of the older sandstone units studied herein, have historically been assigned to the upper part of the Corallian Group (e.g., Sun 1992). We follow the convention of Taylor et al. (2001) in placing all Kimmeridgian–Tithonian strata, which are predominantly siliciclastic, in the Kimmeridge Clay Formation (Fig. 1C). Age-equivalent strata in the Boulonnais outcrops are assigned to a large number of lithostratigraphic units (e.g., Proust et al. 2001; Braaksma et al. 2006) (Fig. 1C). Our focus is on two sandstone units: the Grès de Châtillon and Grès de la Crèche (Figs. 1C, 3). The subsurface succession in southern England and the Boulonnais outcrop succession have both been tied to the same well-established ammonite biozonation (e.g., Wignall 1991; Geyssant et al. 1993; Proust et al. 1995; Gallois 2000; Taylor et al. 2001; Williams et al. 2001; Taylor and Sellwood 2002; Braaksma et al. 2006) (Fig. 1C). Kimmeridgian–Tithonian strata from the Baylei to Fittoni ammonite biozones accumulated over c. 9.7 Myr (Fig. 1C), according to the age model of Ogg and Hinnov (2012) (their Figure 26.8). The duration of each sandstone unit is poorly constrained, but, given the total duration of Kimmeridgian–Tithonian strata, is likely to have been 50–500 kyr.

During the late Jurassic, the Weald Basin was one of a linked chain of intracratonic basins that formed the Laurasian Seaway, which connected the Tethys Ocean to the southeast with the incipient Atlantic Ocean to the northwest (e.g. Ziegler 1989) (Fig. 1A). The basin occupied a paleolatitude of 30–35°N during Kimmeridgian and early Tithonian times and was subject to a warm, humid climate that may have been monsoonal (e.g., Hallam 1984; Sellwood and Valdes 2008; Wignall and Ruffell 1990; Hesselbo et al. 2009; Armstrong et al. 2016). In the Oxfordian, shallow-marine sandstones and carbonates accumulated over much of the Weald Basin (e.g., Brookfield 1973; Bradshaw et al. 1992; Sun 1992). Later, in the Kimmeridgian, accelerated tectonic subsidence due to active extensional of the basin-bounding fault zones resulted in deepening of the basin (Chadwick 1986). At this time, the organic-rich Kimmeridge Clay accumulated over much of the Laurasian Seaway, including the Weald Basin, and thin, shallow-marine sandstones and carbonates fringed the margins of the seaway (Ager and Wallace 1970; Sun 1992; Proust et al. 1995; Wignall et al. 1996; Taylor et al. 2001; Taylor and Sellwood 2002). Coccolith-rich micritic limestones accumulated in the centre of the Weald Basin during the early Tithonian (Taylor et al. 2001; Taylor and Sellwood 2002). The London–Brabant Massif, which defines the northeastern margin of the Weald Basin (Fig. 1B), formed an emergent landmass that was progressively onlapped throughout the Oxfordian and Kimmeridgian (Pharoah 2018). The studied sandstone units are interpreted to have been derived from the London–Brabant Massif (e.g., Ager and Wallace 1970; Proust et al. 1995; Wignall et al. 1996; Taylor and Sellwood 2002), probably from very low-grade metasediments of late Ordovician to early Devonian age that subcrop Oxfordian and Kimmeridgian strata here (cf. Pharoah 2018). Thus, it is likely that sand was transported only a short distance (< 100 km) from the London–Brabant Massif source to the Weald Basin sink (Fig. 1B). Kimmeridgian–Tithonian paleoshorelines are inferred to have been oriented approximately parallel to the southern margin of the London–Brabant Massif, trending approximately west–east in southern England and curving locally to trend approximately north–south in the Boulonnais (Fig. 1B) (Proust et al. 1995; Wignall et al. 1996). The locations of rivers draining the London–Brabant Massif and of riverine sediment input points to Kimmeridgian–Tithonian paleoshorelines are uncertain, due to early Cretaceous erosion over the massif and adjacent areas (Pharoah 2018).

DATA AND METHODS

This study uses publically released data from 50 wells from the onshore southern UK, and four measured sections from outcrops in the Boulonnais region of northern France (Fig. 2). Data collection at outcrop was focussed on two sandstone formations, the Grès de Châtillon and Grès de la Crèche (Figs. 1C, 3). The biostratigraphic context of these formations has been synthesized by Geyssant et al. (1993) from a variety of previous sources and original analyses, and tied to a well-established ammonite biozonation (e.g., Proust et al. 1995). High-resolution, 2D shallow seismic data collected offshore of the outcrops also allow some geometric aspects of stratal configuration to be related to vertical successions exposed at outcrop. Previously published interpretations of these shallow seismic data (Mahieux et al. 1998; Proust et al. 2001; Braaksma et al. 2006) have been re-evaluated as part of our analysis.

Nine wells contain core through Kimmeridgian–Tithonian sandstones (Fig. 2), and all available core, totalling an along-hole thickness of 138 m, was logged. Gamma-ray logs, sonic logs, and cuttings data were used to determine lithology in uncored wells and uncored intervals of cored wells. Caliper logs indicate that borehole conditions were of variable quality in different wells during wireline logging, such that density and neutron logs may not be reliable for lithological interpretation. Well correlations are based on previously published correlations in the Weald Basin (Sun 1992; Hawkes et al. 1998; Taylor et al. 2001; Taylor and Sellwood 2002; Trueman 2003). These previous well correlations are tied to the same ammonite biozonation as is used for the Boulonnais outcrops (Fig. 1C; Gallois 2000; Taylor et al. 2001; Taylor and Sellwood 2002). Correlations are consistent with, but well below the resolution of, 2D seismic data, in which Kimmeridgian–Tithonian strata are represented by laterally continuous, parallel reflectors of variable amplitude that can be traced across the Weald Basin (e.g., Butler and Jamieson 2013). These seismic data are publically available from the UK Onshore Geophysical Library (www.ukogl.org.uk).

Facies analysis of both outcrop and core data is based on observations of lithology, grain size and sorting, sedimentary structures, body fossils, and trace-fossil assemblages. Bioturbation intensity is described using the bioturbation index (BI) of Taylor and Goldring (1993). Paleocurrent data measured at outcrop were corrected for tectonic dip where necessary (e.g. at Cap Gris Nez; Fig. 2).

Sandstone petrography was analyzed using thin sections from 17 samples, which were selected from representative facies of sandstone units at outcrop (8 samples) and in core (9 samples). 300 points were counted in each thin section using the standard procedures of Krumbein and Pettijohn (1938) and Galehouse (1971), in order to measure bulk composition using the Gazzi–Dickinson method (Dickinson 1970), as a first-order indicator of provenance (Dickinson et al. 1983).

FACIES ANALYSIS

Four facies associations have been identified in the studied sandstones and surrounding fine-grained deposits, at outcrop and in core. These facies associations are described and interpreted below, and their vertical stacking into facies successions is then characterized in outcrop and core data (Figs. 4, 5).

Facies Association 1: Mudstones (Offshore and Offshore Transition)

Description.--- Facies Association 1 consists of variably bioturbated claystones and siltstones in successions that are 0.5 to > 11.1 m thick (Figs. 4, 5). Locally the claystone and siltstone successions contain nodular, calcareous siltstone beds (Fig. 6A) and thin (< 3 cm) lenticular and tabular beds of very fine-grained sandstone that contain ripple cross-lamination disrupted by bioturbation (Fig. 6B–D). Bioturbation is moderate to intense (BI: 3–5) in much of the facies association, and is characterized by a diverse assemblage that includes *Planolites*, *Palaeophycus*, *Rhizocorallium*, *Zoophycus*, *Diplocraterion*, *Teichichnus*, *Thalassinoides,* and *Chondrites* (Figs. 4, 5, 6). However, some claystones and siltstones are nonbioturbated (BI: 0) or exhibit bioturbation of sparse to moderate intensity (BI: 1–3) by *Chondrites* and *Planolites*. Claystones and siltstones contain parallel lamination where physical structures are preserved. Fragmented and disarticulated bivalve shells are common throughout the facies association (Fig. 6D), and locally occur as thin (< 10 cm) bioclastic shell beds (e.g., at 1.0 m and 1.3 m in Fig. 4C; at 967.6 m in Fig. 5E). A diverse microfauna characterized by abundant foraminifera and ostracods has been documented in Facies Association 1 in the Boulonnais outcrops (Wignall 1990; Wignall et al. 1996). Facies Association 1 is equivalent to "lithofacies unit 1" of Sun (1992), mudstones and bioclastic mudstones assigned to "outer ramp and mid-ramp deposits" by Proust et al. (1995), "facies 1" of Wignall et al. (1996), "lithofacies 1, 2, and 5-7" of Proust et al. (2001), and "Facies A" of Schlirf (2003). Facies Association 1 overlies Facies Associations 2, 3 and 4 across sharp or, more rarely, gradational contacts, and gradationally underlies Facies Association 2 (Figs. 4, 5).

Interpretation.--- The fine-grained, predominantly siliciclastic character of Facies Association 1 implies a relatively high supply of clay and silt. Bed-scale variations in bioturbation intensity, early-diagenetic calcite cement, and, to an extent, bioclast abundance may reflect variable sedimentation rate (e.g., Ghadeer and MacQuaker 2011; Gingras et al. 2011). The high-diversity trace-fossil assemblage that characterizes most of the facies association constitutes the *Cruziana* ichnofacies, implying deposition in well-oxygenated, open-marine, offshore and offshore-transition environments below effective storm wave base (Pemberton et al. 1992; MacEachern and Bann 2008). Body-fossil assemblages constitute a diverse infaunal and epifaunal bivalve fauna (Wignall et al. 1996) and a diverse nektonic ostracod fauna (Wignall 1990). In contrast, claystone and siltstone intervals characterized by a low-diversity trace-fossil assemblage (*Chondrites*, *Planolites*) were subject to persistent physico-chemical stress during deposition (e.g., Bromley and Ekdale 1984; Savrda and Bottjer 1989; MacQuaker and Gawthorpe 1993; Ghadeer and MacQuaker 2011; Gingras et al. 2011). Thin, ripple cross-laminated, very fine-grained sandstone beds are interpreted to record episodic influxes of sand. Given the close affinity between Facies Associations 1 and 2 (Figs. 4, 5), these sand influxes probably formed in response to anomalously large storms and/or wave-supported sediment gravity flows. Thin, bioclastic shell beds also reflect reworking and winnowing of shells, indicating deposition above effective storm wave base (Fürsich 1986; Proust et al. 1995; Wignall et al. 1996; Schlirf 2003) and condensed sedimentation (Kidwell 1986).

Facies Association 2: Bioturbated and Laminated Silty Sandstones (Lower Shoreface)

Description.--- Facies Association 2 consists of very fine-grained to coarse-grained, moderately to well-sorted sandstones that occur in sharp-based, tabular beds up to 20 cm thick, and that are variably interbedded with siltstones (Figs. 4, 5). Successions of Facies Association 2 are 0.5–6.7 m thick (Figs. 4, 5). Sandstone beds contain charcoal, shell fragments, and mudclasts (Fig. 7E). Medium-grained and coarse-grained sandstone beds are structureless (Fig. 7C), whereas very fine-grained to fine-grained sandstone beds contain parallel lamination, low-angle cross-lamination (Fig. 7F), and hummocky cross-stratification. In their upper part, some sandstone beds contain symmetrical and/or asymmetrical ripple cross-lamination. Sandstone bed tops are moderately to intensely bioturbated (BI: 3–5) by *Thalassinoides*, *Ophiomorpha,* and *Rhizocorallium,* while interbedded siltstones are bioturbated to a similar intensity by *Planolites*, *Palaeophycus*, *Teichichnus*, *Zoophycus*, and *Chondrites* (Fig. 7A–D). These two trace-fossil assemblages overprint each other in intervals of thin-bedded sandstones and siltstones (Fig. 7A, B, D, G). Facies Association 2 is equivalent to "lithofacies units 2 and 4" of Sun (1992), bioturbated sandy shales assigned to "inner ramp deposits" by Proust et al. (1995), "facies 2 and 3" of Wignall et al. (1996), "lithofacies 10 and 11" of Proust et al. (2001), and "Facies B, C, and D" of Schlirf (2003). Facies Association 2 occurs in two contexts in vertical successions. Either it gradationally overlies Facies Association 1 and is sharply overlain by Facies Associations 3, or it overlies Facies Associations 3 and 4 across a sharp contact and is gradationally overlain by Facies Association 1 (Figs. 4, 5).

Interpretation.--- This facies association records episodic influxes of sand, separated by prolonged periods of silt deposition and sediment reworking by bioturbation. The sharp bases of the sandstone beds indicate that they record erosion and subsequent deposition by waning currents. The occurrence of hummocky cross-stratification in very fine-grained to fine-grained sandstone beds implies deposition from oscillatory or combined currents set up during storms (e.g., Duke 1985; Southard et al. 1990; Dumas et al. 2005). Parallel lamination and low-angle cross-lamination in very fine-grained to fine-grained sandstone beds may have resulted from the action of similar currents, although they may also record upper-plane-bed conditions and bedform migration in response to unidirectional currents, respectively (e.g., Bridge and Best 1988; Cheel 1990). The lack of structures in medium-grained and coarse-grained sandstone beds may represent transport of moderately to well-sorted sand as debris flows (e.g., Fisher 1971). In all sandstone beds, rippled tops indicate waning flow velocity. Bioturbation at sandstone bed tops contains elements of the *Skolithos* ichnofacies, reflecting opportunistic colonization of event beds (Pemberton and MacEachern 1997; MacEachern and Bann 2008). The trace-fossil assemblage in interbedded siltstones constitutes the *Cruziana* ichnofacies. Facies Association 2 therefore represents deposition above effective storm wave base but below fairweather wave base, as previously interpreted by Sun (1992), Proust et al. (1995, 2001), Wignall et al. (1996), Schlirf (2003), in the lower-shoreface environment. The presence of charcoal clasts supports deposition in a shallow-marine environment that was close to land. Variability in sandstone-bed thickness and amalgamation in successions of Facies Association 2 is interpreted to reflect a combination of minor variations in water depth, sand supply, and storm-wave climate (Dott and Bourgeois 1982; Storms and Hampson 2005; Sømme et al. 2008).

Facies Association 3: Cross-Bedded Sandstones (Upper Shoreface and Foreshore)

Description.--- Facies Association 3 comprises very fine-grained to very coarse-grained, granular sandstones that contain trough and tabular cross-beds with subordinate planar-parallel-laminated beds (Figs. 4, 5). Successions of the facies association are 0.4–9.5 m thick (Figs. 4, 5). Cross-sets are 5–30 cm thick (Fig. 8C, D, E), and locally contain charcoal, shell fragments, and mudclasts along their bases and foresets (Fig. 8D). There is no apparent vertical trend in cross-set thickness or stacking (Figs. 4, 5). Some cross-sets overlie thin (< 2 cm), structureless or sparsely bioturbated mudstones (Fig. 8B). At outcrop, these mudstones are observed to form laterally discontinuous drapes above trough-shaped erosion surfaces that are 20–50 cm wide, up to 1.5 m long, and variably modified by symmetrical ripples (Fig. 8E, F). Symmetrical ripple crests are either curved, so that they trace out the strike of the underlying trough (Fig. 8F), or they are straight, extend across trough boundaries, and are sub-perpendicular to trough axes (Fig. 8G). Ripple crests are either sharp (Fig. 8E) or rounded (Fig. 8F–H). In addition to fields of parallel, straight-crested ripples (Fig. 8E, F, G), some straight-crested ripples exhibit a lower-wavelength set of ripples superimposed on, and perpendicular to, their troughs (i.e., ladder ripples). Some bedding planes also exhibit two or three sets of symmetrical ripples of similar wavelength with crestlines of different orientation (i.e., interference ripples) (Fig. 8H). Trough and tabular cross-beds exhibit a range of paleocurrent orientations, predominantly towards the southwest and southeast (i.e., obliquely offshore and onshore, respectively), but also towards the north (i.e., alongshore) (Fig. 4) (Wignall et al. 1996). Symmetrical ripple crests strike southwest–northeast and northwest–southeast (i.e., oblique to the paleoshoreline) (Fig. 4) (Wignall et al. 1996). Bioturbation is patchy, and locally absent to moderate in intensity (BI: 0–3). Trace-fossil assemblages in the sandstones are dominated by *Thalassinoides* and *Ophiomorpha* (Fig. 8A, G), with less abundant *Arenicolites* and *Diplocraterion*. Mudstones contain sparse to low-intensity bioturbation by *Planolites*, *Palaeophycus*, and *Thalassinoides* (Fig. 8B). Palynological assemblages characterized by open-marine dincysts have been documented in Facies Association 3 in the subsurface (Sun 1992). Locally, successions of Facies Association 3 are capped by intervals that are pervasively penetrated by rootlets that impart a mottled, subvertical fabric (e.g., at 18.8 m in Fig. 4C; Fig. 8I). At outcrop, the facies association contains isolated, spheroidal calcite-cemented concretions up to 50 cm in diameter (Fig. 4). Calcite-cemented sandstone intervals in core are up to 4.6 m thick (Fig. 5). Facies Association 3 is equivalent to “lithofacies units 3 and 5” of Sun (1992), cross-bedded sandstones assigned to “inner ramp deposits" by Proust et al. (1995), "facies 4-7" of Wignall et al. (1996), "lithofacies 12-14" of Proust et al. (2001), and "Facies E-J" of Schlirf (2003). Facies Association 3 has sharp lower and upper contacts, overlies Facies Association 2, and is overlain by Facies Associations 1, 2 and 4 (Figs. 4, 5).

Interpretation.--- Cross-beds in Facies Association 3 record migration of sinuous- and straight-crested dunes in response to unidirectional currents. The wide range of paleocurrent orientations indicated by trough and tabular cross-beds (Fig. 4) indicates that dunes migrated alongshore, offshore, and onshore (Wignall et al. 1996). Currents were not active continuously, but structureless or sparsely bioturbated mudstones accumulated in the scour pools of migrating dunes, recorded by trough-shaped erosion surfaces, during periods of low flow velocity. The internally structureless character of many mudstones indicates deposition from fluid muds, which result from high concentrations of mud in suspension (Dalrymple et al. 2003). Fluid muds are common in shallow-marine environments with high suspended-mud concentrations due to riverine sediment influx, resuspension of mud by waves (e.g., Traykovski et al. 2000; Lamb and Parsons 2005; Ichaso and Dalrymple 2009), or flocculation where fresh and marine waters mix (Dalrymple et al. 2003). The widespread occurrence of symmetrical ripples at sandstone bed tops indicates wave action, with preservation of the ripples attributed to rapid deposition of overlying, cohesive fluid-mud drapes. Curvature of symmetrical ripple crests along the strike of trough-shaped erosion surfaces indicates wave refraction in shallow water, in response to the localized bathymetric relief of dune scour pools. Wave refraction therefore occurred in shallower water than is required for subsequent dune migration. Ladder and interference ripples record the generation of multiple sets of ripple-crest orientations due to refraction and reflection in similarly shallow water (e.g., Tanner 1960, p. 355–372 in Reineck and Singh 1973). Planar-parallel-laminated beds record upper-plane-bed conditions developed under higher flow velocities than those that generated dunes, possibly in response to breaking waves (cf. Clifton 1976). This latter interpretation of swash–backwash processes is supported by localized overprinting of planar-parallel-laminated sandstones by rootlets, which indicate subaerial exposure. The trace-fossil assemblage in Facies Association 3 constitutes the *Skolithos* ichnofacies, implying deposition in a high-energy, open-marine environment (Pemberton et al. 1992; MacEachern and Bann 2008).

Facies Association 3 is interpreted to record deposition above fairweather wave base (e.g., Sun 1992; Proust et al. 1995, 2001), probably in upper-shoreface and foreshore environments given the localized occurrence of rootlets and charcoal (Wignall et al. 1996; Schlirf 2003). The abundance of cross-bedding, wide range of paleocurrent orientations, and sharp base of successions of Facies Association 3 are all consistent with deposition on a high-energy shoreface containing bars separated by troughs (e.g., Davidson-Arnott and Greenwood 1976; Hunter et al. 1979; Clifton 2006). The interbedding of sandstone cross-sets, structureless or sparsely bioturbated mudstones, wave-rippled surfaces, and planar-parallel-laminated sandstones indicates that fluctuations in flow velocity and water depth were pervasive throughout deposition of vertical successions of Facies Association 3, indicating the action of tides in a shallow subtidal to intertidal setting (Ager and Wallace 1970; Proust et al. 1995, 2001; Schlirf 2003). Proust et al. (1995, 2001) tentatively interpreted Facies Association 3 to contain distinct tidal-bar, tidal-inlet, and tidal-flat deposits in an overall estuarine succession. Alternatively, these characteristics can be attributed to tidal effects on a wave-dominated shoreface (Dashtgard et al. 2009, 2012), particularly one characterized by vertically stacked deposits of subtidal and intertidal bars (cf. Davidson-Arnott and Greenwood 1974, 1976). The latter interpretation is favoured by the consistently sandstone-dominated character of Facies Association 3, which lacks upward-fining, subaerially exposed units that are diagnostic of tidal flats (e.g., p. 355–372 in Reineck and Singh 1973) and deep, channelized scours that are typical of tidal inlets (e.g., Moslow and Tye 1985). The absence of upward-thickening trends in cross-bed thickness in successions of Facies Association 3 also discounts the interpretation of compound tidal dunes, also known as tidal sand waves (Dalrymple and Rhodes 1995; Olariu et al. 2012).

Facies Association 4: Bioclastic Sandstones and Gravels (Transgressive Lag)

Description.--- Facies Association 4 consists of individual and stacked sandstone beds that have thin (1–10 cm) bioclast gravels in their lower part, and that may also contain mudstone interbeds (Figs. 4, 5). Successions of the facies association are 0.1–2.8 m thick (Figs. 4, 5). Bioclasts are predominantly disarticulated thick-shelled bivalves (*Isognomon*, *Gervillella*, *Myophorella*, *Trigonia*, *Nanogyra*), some of which are fragmented (Fig. 9) (Proust et al. 1995, 2001; Wignall et al. 1996; Schlirf 2003). Sandstone beds may contain charcoal clasts (Fig. 9C) and, locally, extrabasinal granules and pebbles (Fig. 9E) in addition to bioclasts. These beds are erosionally based, contain parallel lamination and low-angle cross-lamination, and are sparsely to moderately bioturbated by *Thalassinoides*, *Ophiomorpha, Arenicolites*, *Diplocraterion* and *Planolites* (Figs. 4, 5). Successions of Facies Association 4 are commonly calcite cemented, although cementation does not typically extend into underlying deposits (Figs. 4, 5). Facies Association 4 is equivalent to shell layers and shell lags assigned to “mid-ramp and inner ramp deposits” by Proust et al. (1995), “facies 8” of Wignall et al. (1996), “lithofacies 6 and 8” of Proust et al. (2001), and “Facies J2 and K” of Schlirf (2003). Facies Association 4 overlies Facies Associations 1, 2, and 3 across a sharp contact (Figs. 4, 5), which may be associated with unlined *Thalassinoides* that are infilled by coarse-grained, bioclastic sandstone from the overlying unit (Fig. 9D). Facies Association 4 is overlain by Facies Associations 1 and 2 (Figs. 4, 5).

Interpretation.--- Bioclastic gravels in Facies Association 4 are interpreted as winnowed lags, in which large, dense clasts have been concentrated by strong current reworking and removal of sand and mud. The disarticulated and fragmented character of the bioclasts implies that they may also have been transported. The sharp base of Facies Association 4 is consistent with erosion and reworking of the underlying substrate. Unlined, passively infilled *Thalassinoides* associated with these surfaces constitute the *Glossifungites* ichnofacies, implying erosional exhumation of a consolidated substrate at a firmground (MacEachern et al. 1992; Pemberton et al. 1992). The bioclastic gravels are associated with sandstone beds and mudstone interbeds that are similar to those in Facies Association 2, and which are also interpreted as storm-event beds separated by fairweather deposits. Given their vertical stratigraphic context, units of Facies Association 4 are interpreted as offshore (Facies Association 1) and shoreface deposits (e.g. Facies Associations 2 and 3) that were erosionally reworked by storm waves (Wignall et al. 1996). The local occurrence of extrabasinal granules in Facies Association 4 implies that bedrock outcrops from the basin margins were also erosionally reworked to provide sediment that was then transported basinward (Wignall et al. 1996). The stratigraphic significance of the erosional bases of units of Facies Association 4 is considered below, in the context of vertical facies successions. Calcite cements are microcrystalline, with textures and oxygen and carbon isotopic compositions that imply early cementation from marine pore waters (Al Ramadan et al. 2005).

Facies Successions

Description.--- The facies associations described above are arranged into two recurring types of vertical facies succession. The first type is characterized by an overall upward-coarsening trend in grain size, and consists of mudstones (Facies Association 1) passing gradationally upward into bioturbated and laminated silty sandstones (Facies Association 2) that are sharply overlain by cross-bedded sandstones (Facies Association 3) (successions represented by upward-widening triangles in Figs. 4, 5). The sharp bases of the cross-bedded sandstones (Facies Association 3) have a planar geometry and low erosional relief (typically several centimeters at outcrop), but mark a more pronounced change in facies than the bases of individual sandstone beds in Facies Association 2. Some successions of this type are incomplete, and lack either mudstones (Facies Association 1) in their lower part (e.g., 1090.0–1083.2 m in Fig. 5A) or cross-bedded sandstones (Facies Association 3) in their upper part (e.g., 0–1.9 m in Fig. 4D; 1033.4–1026.0 m in Fig. 5B, 965.0–951.9 m in Fig. 5E). Upward-coarsening facies successions are 4.7–15.9 m thick (Figs. 4, 5).

The second type of vertical facies succession exhibits an overall upward-fining trend in grain size, and consists of bioturbated and laminated silty sandstones (Facies Association 2) that pass gradationally upward into mudstones (Facies Association 1) (successions represented by upward-thinning triangles in Figs. 4, 5). Bioclastic sandstones and gravels (Facies Association 4) occur locally at the base of (e.g., 4.9–5.2 m in Fig. 4B) and within these successions (e.g., 970.9–968.6 m in Fig. 5E). Upward-fining facies successions are 0.2–8.5 m thick (Figs. 4, 5).

Interpretation.--- Upward-coarsening facies successions, consisting of Facies Association 1 overlain by Facies Association 2 and then Facies Association 3, are interpreted to record upward shallowing and regression. In this context, the sharp base of Facies Association 3 can be attributed either to migration of troughs between bars on a high-energy shoreface (e.g., Hunter et al. 1979; Clifton 2006), or to wave erosion during falling relative sea level, which generated a regressive surface of marine erosion at the base of a "sharp-based shoreface" (*sensu* Plint 1988) (Proust et al. 1995, 2001; Wignall et al. 1996).

Upward-fining facies successions, consisting of Facies Association 2 overlain by Facies Association 1, are interpreted to record upward deepening and transgression. Bioclastic sandstone and gravel lags (Facies Association 4) at the base of, and within, such successions are interpreted to line wave ravinement surfaces (*sensu* Swift 1968) cut by wave action during shoreface retreat. However, bioclastic lags may also occur at the base of individual storm-event beds in Facies Association 2, as noted in other bioclastic-rich sandstones (e.g., Kantarowicz et al. 1987; Morris et al. 2006). The tops of upward-fining facies successions occur within mudstones of Facies Association 1, and are interpreted as flooding surfaces (Proust et al. 1995, 2001).

We also note that, although not the focus of this paper, thin, condensed, bioclastic shell beds within offshore and offshore-transition mudstones (Facies Association 1) have been interpreted previously as very closely spaced or composite wave ravinement and flooding surfaces (e.g. "marine starvation surfaces" of Wignall et al. 1996; "condensed section systems tracts" of Braaksma et al. 2006). This interpretation is consistent with interpretations of similar units (e.g., Kidwell 1986; Föllmi 2016), and implies a distal location for the composite wave ravinement and flooding surfaces, given their juxtaposition above and below offshore and offshore-transition deposits. The interpretation is yet to be tested by correlation of the thin, condensed, bioclastic shell beds into more proximal locations.

Stratal Geometries in Shallow, High-Resolution Seismic Data

Description.--- Upward-coarsening facies successions are resolved in high-resolution 2D seismic (sparker) data to contain dipping clinoform surfaces that extend from the base to the top of the succession (e.g., in the Grès de Châtillon to the west of the Pointe du Nid de Corbet; Fig. 10A). Clinoforms appear to be linear in cross-sectional geometry, with relatively uniform apparent dip, in seismic lines oriented approximately perpendicular (Fig. 10A, B) and parallel (Fig. 10C) to the paleoshoreline (Figs. 1B, 10D). However, apparent dips vary with the orientation of the 2D seismic line, as would be expected, and potentially with stratigraphic unit (e.g., apparent 1˚ dip to the west, approximately perpendicular to the paleoshoreline, in the Grès de Châtillon, Fig. 10A; apparent 5–10˚ dips to the north, approximately parallel to the paleoshoreline, in the Grès de la Crèche, Fig. 10C). Clinoforms are truncated by planar surfaces (dashed blue lines in Fig. 10A, B) that display locally channelized erosional relief (dashed blue line in Fig. 10C), and downlap planar surfaces (dashed red lines in Fig. 10A–C). Locally, the Grès de la Crèche contains two vertically stacked clinoform sets with the characteristics described above (corresponding to the Lower and Upper Grès de la Crèche units of Proust et al. 2001), separated by a unit of parallel, high-amplitude reflectors (corresponding to the Marnes Intercalaires unit of Proust et al. 2001) (Fig. 10B). Also in the Grès de la Crèche, several of these clinoforms are downlapped by or truncate smaller, laterally discontinuous, superimposed clinoform sets with steep internal apparent dips (up to 10˚) (Fig. 10C). A few of the larger, through-going clinoforms are also marked by subtle truncation related to an angular discordance in clinoform dip (Fig. 10B, C).

Upward-fining facies successions are resolved as sets of parallel reflectors (e.g., in the Grès de Châtillon to the west of the Pointe du Nid de Corbet; Fig. 10A). The successions overlie top-truncated clinoforms across a planar to locally channelized erosion surface (dashed blue lines in Fig. 10A–C), and are capped by a parallel reflector (solid blue line in Fig. 10A).

Interpretation.--- The occurrence of a single clinoform set extending from the base to the top of each upward-coarsening facies succession supports their interpretation as regressive shoreface deposits. Clinoforms dip offshore (Fig. 10A, B) and also subparallel to the paleoshoreline (Fig. 10C). The combination of offshore-directed and alongshore-directed progradation of clinoforms in a shoreface succession can potentially be attributed to accretion on: (1) the margin of a laterally migrating rip channel in a barred, high-energy shoreface (e.g., Hunter et al. 1979; Clifton 2006); (2) a spit fronted by a shoreface (e.g., Nielsen et al. 1988); or (3) a shoreline-attached tidal bar (cf. Dalrymple et al. 2003; Olariu et al. 2012) with a wave-reworked shoreface at its front. The erosion surfaces that truncate these clinoform sets (dashed blue lines in Fig. 10A–C) are overlain by an upward-fining, transgressive facies succession (e.g., Fig. 10A) or by another upward-coarsening, regressive facies succession (e.g., Fig. 10B). The erosion surfaces are associated with transgression, and the planar geometry of most surfaces is consistent with their interpretation as wave ravinement surfaces (*sensu* Swift 1968). Local channelized erosion at the surfaces (e.g., Fig. 10C) is attributed to scour during transgression, possibly by tidal inlets or channels (Braaksma et al. 2006). Where upward-fining, transgressive facies successions are resolved, they are interpreted to be capped by flooding surfaces (solid blue line in Fig. 10A).

Small, laterally discontinuous clinoform sets that are superimposed on the regressive shoreface clinoforms are interpreted as bars; the common apparent dip direction of clinoforms at both scales (Fig. 10C) implies that the bars migrated down the clinoform and subparallel to the paleoshoreline. This hierarchical arrangement and orientation of cross-stratification is consistent with deposition on the margin of a laterally migrating rip channel in a barred, high-energy shoreface (e.g., Hunter et al. 1979; Clifton 2006) or the distal tip of a spit (e.g., Nielsen et al. 1988). However, this geometric configuration is not consistent with a shoreline-attached tidal bar, in which clinoforms at the scale of the tidal bar record lateral accretion, and superimposed cross-strata record perpendicular, offshore-directed dune migration (cf. Dalrymple et al. 2003; Olariu et al. 2012). Locally, bar clinoform sets are vertically stacked within the same shoreface clinoform set (Fig. 10C). Subtle truncation and angular discordance across some through-going, shoreface clinoforms (Fig. 10B, C) is interpreted to reflect localized shoreline reorientation and/or readjustment of the shoreface profile (e.g., Hampson et al. 2008; Sømme et al. 2008; Isla et al. 2018).

Erosion surfaces at the base of shoreface clinoform sets (dashed red lines in Fig. 10A–C) are inferred to correspond to the sharp bases of units of Facies Association 3 in upward-coarsening, regressive facies successions (Figs. 4, 5). As noted in the interpretation of facies successions, these erosional surfaces can be interpreted either as the stratigraphic expression of migrating troughs in a barred, high-energy shoreface (Hunter et al. 1979; Clifton 2006), or as regressive surfaces of marine erosion cut by wave erosion during falling relative sea level (Proust et al. 1995, 2001; Wignall et al. 1996).

Expression in Wireline-Log Data

The two types of facies succession documented above are also imaged in conventional wireline-log data, most consistently within gamma-ray logs (Fig. 11B, C). Upward-coarsening facies successions are represented by an upward-decreasing gamma-ray trend, reflecting an overall upward decrease in clay content, and upward-fining facies successions are represented by an upward-increasing gamma-ray trend, reflecting an overall upward increase in clay content (e.g., cored intervals of individual wells in Fig. 11B, C). Typically, upward-fining facies successions are relatively thin and poorly expressed in the gamma-ray logs, such that many upward-coarsening facies successions appear to have sharp tops at the resolution of the logs. Individual facies associations also cannot be consistently distinguished in the wireline-log data. Thus, regressive–transgressive tongues bounded by interpreted flooding surfaces, which are marked by high gamma-ray values, are the smallest stratal units that can be consistently identified with confidence in wireline-log data (Fig. 11B, C).

Correlation of regressive–transgressive tongues and their bounding flooding surfaces is based on identification of patterns and markers in the gamma-ray logs (e.g., Taylor et al. 2001). Figure 11B and C shows two such correlations in the Weald Basin, based on previously published well correlations (Sun 1992; Taylor et al. 2001; Taylor and Sellwood 2002; Trueman 2003) and calibrated to core (Fig. 5). Regressive–transgressive tongues are correlated to have large lateral extent, comparable to that of regressive–transgressive tongues in the Boulonnais outcrops (Fig. 11A; after Proust et al. 2001), and their bounding flooding surfaces are interpreted to be basinwide (cf. Taylor et al. 2001; Taylor and Sellwood 2002).

FACIES MODEL

The interpretations presented above for Facies Associations 1–3, upward-coarsening facies successions, and clinoform-bearing stratal geometries are synthesized into a facies model of a high-energy, tidally modulated, barred shoreface developed under either an ascending regressive (i.e. normal regressive) or a descending regressive (i.e., forced regressive) shoreline trajectory (*sensu* Helland-Hansen and Martinsen 1996) (Fig. 12B, C). The model comprises three facies belts, each corresponding to a facies association, that represent the following subenvironments, from distal to proximal: (1) offshore and offshore transition, (2) lower shoreface, and (3) upper shoreface and foreshore.

Shoreface Morphology

High-resolution shallow seismic data show that shoreface deposits are characterized by steeply dipping clinoforms (up to 10°), on which are superimposed laterally discontinuous, smaller-scale clinoform sets (Fig. 10C) that dip down the shoreface clinoforms, and are interpreted to represent migrating bars that were separated by troughs (Fig. 12B, C). Clinoform dip directions indicate offshore-directed and alongshore-directed progradation of the shoreface, probably due to lateral migration of rip channels in the shoreface (e.g., Hunter et al. 1979; Clifton 2006) or to accretion along recurved, shoreface-fronted spits (Fig. 12A; e.g., Nielsen et al. 1988). Bar deposits are most evident and abundant in the upper part of thick shoreface clinoform sets (c. 12 m locally in Grès de la Crèche, Fig. 10C; Braaksma et al. 2006), but occur locally in the lower part of the same thick shoreface clinoform sets (Fig. 10C), implying that the shoreface at times contained both inner-bar and outer-bar systems (cf. Davidson-Arnott and Greenwood 1976). Trough and tabular cross-bedded sandstones that correspond to these bar deposits exhibit a wide range of paleocurrent directions, implying that dunes migrated alongshore, offshore, and onshore (Wignall et al. 1996) over the bars and adjacent troughs, and potentially through shoreline-perpendicular or shoreline-oblique rip channels that dissected the bars (cf. Davidson-Arnott and Greenwood 1974, 1976) or around the recurved tips of spits (Fig. 12A; cf. Nielsen et al. 1988; Fruergaard et al. 2020). Stratal geometries consistent with stacking of dune cross-sets to form bar cosets are not noted at outcrop, implying that the stratal relationships resolved in thick shoreface clinoform sets (Fig. 10C) may be more subtly expressed, or absent, in the thinner shoreface deposits typical of the Boulonnais outcrops (Fig. 4). However, surfaces marked by straight wave-ripple crests that extend across dune-scale trough boundaries (Fig. 8G) may represent the remnants of poorly preserved bar morphologies. The lateral migration of troughs between bars may also account for the sharp bases of cross-bedded, upper-shoreface and foreshore sandstones (Facies Association 3) (Hunter et al. 1979; Clifton 2006). The occurrence of steep shoreface clinoforms and shoreface bar systems implies high fairweather-wave energy (Clifton 2006), in contrast to moderate fairweather-wave energy, which results in more gently dipping shoreface profiles (c. 0.5˚) and the generation of wave-modified, symmetrical, dune cross-bedding in shoreface deposits (Vaucher et al. 2017, 2018).

Tidal Influence

As noted previously, two features of cross-bedded, upper-shoreface and foreshore sandstones (Facies Association 3) can potentially be attributed to tidal influence, although this is not a unique interpretation: (1) the occurrence of structureless and sparsely bioturbated mudstone drapes, indicating fluid-mud deposition during periods of low flow velocity; (2) the abundance of wave ripples that record refraction and interference in erosional troughs implies repeated fluctuations in water depth typical of an intertidal setting (Proust et al. 1995, 2001; Schlirf 2003). Although these and other characteristics of the cross-bedded, upper-shoreface and foreshore sandstones (Facies Association 3) are noted in modern shorefaces developed under a large tidal range, including those fronting spits (e.g., Fruergaard et al. 2020), they do not provide the direct evidence of strong tidal currents that typifies tide-influenced shorefaces (Dashtgard et al. 2012). The repeated interbedding of structures generated by swash–backwash (planar-parallel lamination), surf and breaking waves (trough and tabular cross-beds), and shoaling waves (wave ripples) in deposits of the upper-shoreface and foreshore facies belt is consistent with regular variations in water depth during a tidal cycle on a tidally modulated shoreface (Dashtgard et al. 2009, 2012) (Fig. 12B, C). Upper shoreface and foreshore deposits form a large proportion of the overall thickness of regressive shoreface-sandstone successions (42–78% at outcrop, Fig. 4; 32–93% in core, Fig. 5), which may indicate that upper-shoreface and foreshore deposits were "overthickened" as a result of a high tidal range (Dashtgard et al. 2012). The correspondingly small relative thickness of lower-shoreface deposits and scarcity of well-preserved hummocky cross-stratified beds implies low storm-wave energy, high tidal energy, or limited sand supply.

Sequence Stratigraphic Variations on Facies Model

The facies model described above and presented in Figure 12B assumes an ascending regressive (i.e. normal regressive) shoreline trajectory (*sensu* Helland-Hansen and Martinsen 1996). In this model, the sharp bases of cross-bedded, upper-shoreface and foreshore sandstone units (Facies Association 3) are attributed to lateral migration of bars on a high-energy shoreface (Hunter et al. 1979; Clifton 2006). Alternatively, the sharp bases of these sandstone units may have resulted from wave erosion during falling relative sea level, which generated a regressive surface of marine erosion at the base of a "sharp-based shoreface" (*sensu* Plint 1988) (Fig. 12C; Proust et al. 1995, 2001; Wignall et al. 1996). The latter mechanism requires that the angle of descending regressive (i.e., forced regressive) shoreline trajectory (*sensu* Helland-Hansen and Martinsen 1996) was steeper than the angle of shoreface–shelf dip at wave base (Cant 1991). This geometric condition is unlikely to have been met for large progradation distances (greater than several kilometers), since it requires a high-magnitude relative sea-level fall that continually outpaced progradation driven by sediment supply (e.g., Hampson 2000). However, the thin, laterally extensive geometry of the shoreface sandstones and the absence of coastal-plain deposits (Fig. 11) are both consistent with shoreface progradation under a net-descending regressive shoreline trajectory, which may have been punctuated by intervals of ascending regressive shoreline trajectory (i.e., alternation of the shoreline trajectories shown in Fig. 12B and C), particularly if combined with subsequent transgressive erosion (cf. Plint 1988). Patterns of carbonate-grain dissolution and concomitant carbonate cementation in the Grès de Connincthun, Grès de Châtillon, and Grès de la Crèche are also consistent with the incursion of meteoric waters during relative sea-level fall during progradation of each sandstone unit (Al-Ramadan et al. 2015).

During transgression, only the distal components of the facies model are preserved, in the form of an upward-deepening succession that comprises lower-shoreface deposits overlain by offshore and offshore-transition deposits (Fig. 12B, C). Such successions are bounded at their base by surfaces that record transgressive erosion by waves during shoreface retreat (i.e., wave ravinement surfaces), and at their top by surfaces that record maximum water depth (i.e., flooding surfaces) (Figs. 4, 5).

STRATIGRAPHIC AND PALEOGEOGRAPHIC CONTEXT

Tidally modulated shorefaces, such as those interpreted above, are inferred to develop preferentially in embayments and epicontinental seaways, where tidal amplification is pronounced but wave energy is low to moderate (Dashtgard et al. 2012; Vaucher et al. 2017). Below, we evaluate the stratigraphic framework and paleogeographic distribution of the studied Kimmeridgian–Tithonian sandstones. This contextual information is then used in combination with previously published tidal-modelling results for the Laurasian Seaway (Fig. 1A) to assess the potential for appropriate wave and tide conditions for the development of tidally modulated shorefaces in the Weald Basin (Fig. 1B).

Sequence Stratigraphic Framework

Sandstones in the Boulonnais region are correlated between outcrop measured sections using the framework of Proust et al. (2001), which uses offshore, high-resolution seismic data (e.g., Fig. 10) and biostratigraphic data to interpret stratal relationships that are not exposed in the onshore outcrop belt, which is folded and faulted (Bonte et al. 1985; Mansy et al. 2007) (Fig. 11A). The large lateral extent (> 25 km) and continuous, sheet-like geometry of regressive–transgressive tongues bounded by flooding surfaces in the Boulonnais outcrop belt (Fig. 11A) have been used to guide correlation of regressive–transgressive sandstone tongues between wells in the subsurface of southern England (Fig. 11B, C).

Our subsurface correlation panels have been adapted from those previously published by Taylor et al. (2001) and Taylor and Sellwood (2002) for Kimmeridgian strata in the Weald Basin (Fig. 11B, C).

Flooding surfaces that bound regressive–transgressive sandstone tongues in the subsurface Weald Basin are numbered based on the sequence stratigraphic nomenclature of Taylor et al. (2001) and Taylor and Sellwood (2002) (Fig. 1C). The regressive–transgressive sandstone tongues in neither the subsurface Weald Basin nor the Boulonnais region coincide consistently with the high-frequency, "third-order" sequence boundaries interpreted by Taylor et al. (2001) and Taylor and Sellwood (2002) (Fig. 1C), despite their potential association with deposition during periods of falling relative sea level (Proust et al. 2001). It is notable that the regressive–transgressive sandstone tongues in the Boulonnais outcrops do not consistently occur at the same stratigraphic levels as those in the subsurface Weald Basin (Wignall 1991) (Fig. 1C). These observations suggest that the detailed, high-frequency stratigraphic and paleogeographic distribution of regressive–transgressive sandstone tongues is strongly influenced by local controls, although the sandstone-bearing succession from the Baylei to Scitulus chronozones (Fig. 1C) exhibits an overall, low-frequency retrogradational stacking pattern (Taylor et al. 2001; Taylor and Sellwood 2002), which is consistent with progressive onlap onto the London–Brabant Massif. The short distance (< 100 km) of sediment routing from the London–Brabant Massif source to the Weald Basin sink (Fig. 1B) may have aided the transfer of high-frequency sediment-supply signals from the sediment source, for example due to local variations in topographic relief or bedrock erodability, into shallow-marine stratigraphic patterns (e.g., Paola et al. 1992; Romans et al. 2016).

Paleogeographic Distribution and Provenance

Each of the regressive–transgressive sandstone tongues forms a west-northwest to east-northeast belt that fringes the southern margin of the London–Brabant Massif (Fig. 13) (cf. Bradshaw et al. 1992; Proust et al. 1995; Wignall et al. 1996). Although the sandstones contain some carbonate grains, in the form of variably reworked bioclasts (Fig. 14B–D), their bulk detrital composition implies a quartzose recycled-orogen provenance (Fig. 14A) (cf. Dickinson et al. 1983). This composition supports derivation from late Ordovician to Lower Devonian sandstones and mudstones of the London–Brabant Massif, which were subjected to very low-grade metamorphism during the late Caledonian Orogeny (Pharoah 2018).

Sandstone detrital grains are subrounded (Fig. 14B–D), implying extended physical reworking before deposition. This inference is supported by the occurrence of authigenic glauconite grains (Fig. 14B, C), which indicate reworking in a shallow-marine setting characterized by low sedimentation rates (e.g., Cloud 1955; Gaynor and Swift 1988). The narrow range of sandstone detrital compositions (Fig. 14A) implies that there was little spatial variation in the lithology of eroded sediment that was ultimately deposited along the shoreline. Grain-size variability in the same facies association between different outcrop and well locations (e.g., compare Fig. 14B and Fig. 14D) is attributed to alongshore variations in: (1) proximity to fluvial sediment input points to the shoreline; (2) proximity to (wave-eroded?) coastal headlands that supplied sediment to the shoreline; (3) grain-size distribution of sediment supply; and (4) the velocity of wave-generated longshore currents and tidal currents. Similar parameters are inferred to have controlled localized variations in the dip extent of the sandstone belt fringing the London–Brabant Massif (Fig. 13). For example, areas of large sandstone dip extent may be characterized by: (1) high local sand supply from an extrabasinal fluvial source or a reworked, intrabasinal marine source; and/or (2) low accommodation due to unusually shallow local water depth or slow subsidence, reflecting fault-related uplift (e.g., Sun 1992; Mansy et al. 2003) or elevated paleotopography of the London–Brabant Massif.

Potential for Tidal Amplification and Low to Moderate Wave Energy

Tidal modelling demonstrates that during the Early Jurassic the tidal wave propagated from the Tethys Ocean into the Laurasian Seaway (Fig. 15A) (Mitchell et al. 2011). Model results indicate that the seaway was regionally microtidal (tidal range of < 2 m), with mesotidal (tidal range of 2–4 m) and macrotidal (tidal range of > 4 m) conditions developed in localized embayments and areas of shoaling close to the Tethys Ocean (Mitchell et al. 2011). The regional tidal range is relatively insensitive to changes in water depth in the Laurasian Seaway, although the latter controls the precise location of funnelling through straits and shoaling over areas of shallow water depth, which can lead to local amplification of tidal range or to locally elevated tidal-current velocities (Mitchell et al. 2011). The Kimmeridgian–Tithonian paleogeography and paleobathymetry of the Laurasian Seaway are similar to those modelled by Mitchell et al. (2011) for the Lower Jurassic seaway, such that the same general results are likely to hold true.

The length scale of rotational movement of the tidal wave due to Coriolis acceleration is termed the Rossby Radius, R, which is approximated by the relationship

$$R = \sqrt{(gh)} / (2\Omega \sin ø) \qquad (1)$$

in which g is the acceleration due to gravity (9.81 $m.s^{-2}$), h is the depth of the water column (m), Ω is the rotation rate of the Earth (7.27×10^{-5} $rad.s^{-1}$), and $ø$ is the latitude (e.g., Cushman-Roisin 1994). The Kimmeridgian–Tithonian Laurasian Seaway occupied a paleolatitude of 35–40°N and was 50–100 m deep, suggesting that parts of the seaway that exceeded 400–800 m (i.e., $2R$) in width contained clockwise-circulating cells that rotated about amphidromic points. The Weald Basin was too narrow to contain one of these cells (Fig. 15B), implying that banking of the rotating tidal wave up against the northeastern shoreline of the Weald Basin is unlikely to have amplified tidal range here.

Tidal amplification takes place in an embayment when its dimensions are in resonance with the quarter wavelength of the tidal wave according to the relationship (Pugh 1987; Sztanò and De Boer 1995)

$$l = \tfrac{1}{4}T\sqrt{(gh)} \qquad (2)$$

in which l is the length of the embayment, and T is the period of the tidal wave (12.42 hours for the principal semidiurnal lunar tidal constituent, M2). The northeastern shoreline of the Weald Basin is reconstructed to define a broad open embayment 150–200 km wide (Figs. 1B, 15B), implying that water depths of 18–33 m would have been required for resonance of semidiurnal tides. Such water depths are consistent with the thickness range of regressive–transgressive sandstone tongues (4–16 m; Figs. 4, 5), particularly when the latter are decompacted. In contrast, tidal resonance in a narrower (c. 50 km) embayment in the Boulonnais area would require a water depth of c. 2 m. Thus, tidal resonance in a broad embayed shoreline is a plausible mechanism to account for amplified tidal range in the northeastern Weald Basin.

The studied shoreline deposits also contain evidence for fairweather- and storm-wave processes, which requires that shorelines along the northeastern Weald Basin were open to wave energy. Paleoclimate models indicate that the prevailing wind direction varied seasonally between westerly (i.e., from west to east) and southwesterly (i.e., from southwest to northeast), and that these winds originated at a paleolatitude of 30°N as part of Hadley-cell circulation (Sellwood and Valdes 2008; Armstrong et al. 2016). These models imply a fetch of 200–600 km for waves reaching the northeastern margin of the Weald Basin (Fig. 15A). In the Wessex Basin, which lies adjacent to and south-southwest of the Weald Basin (Figs. 1B), the occurrence of highly organic-rich shales in the

Kimmeridge Clay is attributed to temporary stratification of the shallow (< 200 m) water column (Tyson et al. 1979; Wignall 1989). Graded, laminated beds and coccolith-rich laminae, which indicate well-mixed, oxygenated waters, in the Kimmeridge Clay of the Wessex Basin are attributed to storm events (Wignall 1989; Macquaker and Gawthorpe 1993; Pearson et al. 2004). By implication, fairweather wave base was shallow, consistent with the small thickness (0.4–9.5 m) of upper-shoreface and foreshore deposits (Figs. 4, 5) and temporary stratification of the water column, but maximum storm wave base was much deeper, extending to the basin floor during major storms. The small thickness of lower-shoreface sandstones (0.5–6.7 m; Figs. 4, 5) relative to the interpreted deep effective storm wave base is attributed to limited sand availability rather than limited storm-wave transport capacity. The interpretations outlined above are consistent with the development of wave-dominated shorefaces at the margins of the Wessex and Weald basins.

CONCLUSIONS AND IMPLICATIONS

Kimmeridgian–Tithonian shallow-marine sandstones from the Weald Basin (southern England and northern France) occur as thin (5–24 m), laterally extensive (tens of kilometers), regressive–transgressive tongues that are interpreted as the deposits of high-energy, tidally modulated, wave-dominated, barred shorefaces. The sandstone tongues fringe the northeastern margin of the Weald Basin, which formed part of the intracratonic Laurasian Seaway that connected the Tethys Ocean to the southeast with the incipient Atlantic Ocean to the northwest. The sedimentologic character of these sandstone tongues is documented in order to extend the range of facies models for mixed-influence shallow marine deposits, and to understand the paleogeographic and stratigraphic context in which they occur.

The lower, regressive part of each sandstone tongue comprises, from base to top: (1) mudstones that are, in general, moderately to intensely bioturbated by a diverse *Cruziana* ichnofacies, which represent offshore to offshore-transition deposits; (2) hummocky cross-stratified, very fine- to fine-grained sandstone beds and mudstone interbeds that are moderately to intensely bioturbated by a mixed *Skolithos* and *Cruziana* ichnofacies, which represent subtidal lower-shoreface deposits; and (3) cross-bedded, medium- to coarse-grained sandstones that are sparsely to moderately bioturbated by a low-diversity *Skolithos* ichnofacies, and that contain mudstone drapes, mudclast lags and wave-rippled surfaces; these cross-bedded sandstones represent shallow subtidal and intertidal deposition on the upper shoreface and foreshore. The interbedding of sandstone cross-beds, mudstone drapes, wave-rippled surfaces (including interference ripples), and planar-parallel-laminated sandstones in upper-shoreface and foreshore sandstones is attributed to pervasive fluctuations in flow velocity and water depth that were modulated by tides. Steeply paleoseaward- and alongshore-dipping (1–10°) clinoforms extend through the regressive part of the shoreface tongues, indicating shoreface progradation and accretion on the margins of laterally migrating rip channels or the tips of recurved, shoreface-fronted spits. Smaller, superimposed clinoform sets in upper-shoreface sandstones are interpreted as bar deposits, indicating a barred-shoreface morphology. The upper, transgressive part of each sandstone tongue comprises an erosionally based bioclastic lag overlain by lower shoreface sandstones that pass upwards into offshore mudstones.

The resulting facies model contains three of the diagnostic features proposed previously for tidally modulated shorefaces: (1) shoreface facies successions are characterized by pervasive interbedding of sedimentary structures that indicate different, depth-dependent wave processes; (2) upper-shoreface and foreshore deposits are "overthickened"; and (3) lower-shoreface deposits contain a mixture of *Skolithos* and *Cruziana* ichnofacies. Potential indicators of direct tidal influence are limited to mudstone drapes in upper-shoreface sandsones. In contrast to previous facies models for tidally modulated shorefaces, upper-shoreface deposits have a sharp, rather than gradational, base that is marked by downlap of shoreface clinoforms. Downlap and the occurrence of paleoseaward- and alongshore-dipping shoreface clinoforms are attributed to the three-dimensional morphology of the shoreface (e.g., presence of longshore bars and troughs, and shoreline-perpendicular to shoreline-oblique rip channels) and the coastal landforms that are fronted by the shoreface (e.g., spits). Current facies models for tidally modulated shorefaces assume a simple linear shoreline, and thus need to be modified to accommodate alongshore variability in shoreline morphology and sediment transport.

Published paleogeographic reconstructions, and climate-model and ocean-model simulations, indicate that the northeastern margin of the Weald Basin formed a broad (150–200 km) embayment that was exposed to an energetic wave climate driven by westerly and southwesterly winds with a fetch of 200–600 km and to the tidal wave that propagated northwestwards from the Tethys Ocean. The development of tidally modulated shorefaces in this embayment probably records resonant amplification of semidiurnal tides, implying shallow water depths (18–33 m) that are consistent with observed sandstone tongue thicknesses.

Estimation of Rossby radius (as a proxy for the potential occurrence of amphidromic cells), potential tor tidal resonance, and potential wave fetch can be applied to other case studies as a tool to predict the spatio-temporal distribution of tidally modulated shorefaces. This approach requires reconstructions of paleogeography and paleobathymetry that constrain paleolatitude, seaway width, embayment length, and water depth. The resulting predictions indicate the potential for tidally modified shorefaces to be developed, and sensitivity associated with this potential.

ACKNOWLEDGMENTS

The authors gratefully acknowledge funding and support from UK Oil & Gas plc, and in particular Stephen Sanderson and Robert Wallace. We thank the British Geological Survey for providing access to core material. We are grateful for the constructive review and editorial comments of an anonymous reviewer, Piret Plink-Björklund, Jennifer Aschoff, and Peter Burgess.

REFERENCES

AGER, D.V., AND WALLACE, P., 1970, The distribution and significance of trace fossils in the uppermost Jurassic rocks of the Boulonnais, northern France, *in* Crimes, T.P., and Harper, J.C., eds., Trace Fossils: Geological Journal, Special Issue 3, p. 1-18.

AINSWORTH, R.B., FLINT, S.S., AND HOWELL, J.A., 2008, Predicting coastal depositional style: influence of basin morphology and accommodation to sediment supply within a sequence stratigraphic framework, *in* Hampson, G.J., Steel, R.J., Burgess, P.M., and Dalrymple, R.W., eds., Recent Advances in Models of Siliciclastic Shallow-Marine Stratigraphy: SEPM, Special Publication 90, p. 237-264.

AINSWORTH, R.B., VAKARELOV, B.K., AND NANSON, R.A., 2011, Dynamic spatial and temporal prediction of changes in depositional processes on clastic shorelines: toward improved subsurface uncertainty reduction and management: American Association of Petroleum Geologists, Bulletin, v. 95, p. 267-297.

AL-RAMADAN, K., MORAD, S., PROUST, J.N., AND AL-AASM, I., 2005, Distribution of diagenetic alterations in siliciclastic shoreface deposits within a sequence stratigraphic framework: evidence from the Upper Jurassic, Boulonnais, NW France: Journal of Sedimentary Research, v. 75, p. 943-959.

ANDREWS, I.J., 2014, The Jurassic shales of the Weald Basin: geology and shale oil and shale gas resource estimation: British Geological Survey for Department of Energy and Climate Change, London, UK, 79 p.

https://www.gov.uk/government/uploads/system/uploads/attachment_data/file/313701/BGS_DECC_JurassicWealdShale_study_2014_MAIN_REPORT.pdf

Armstrong, H.A., Wagner, T., Herringshaw, L.G., Farnsworth, A.J., Lunt, D.J., Harland, M., Imber, J., Loptson, C., and Atar, E.F., 2016, Hadley circulation and precipitation changes controlling black shale deposition in the Late Jurassic Boreal Seaway: Paleoceanography, v. 31, p. 1041-1053.

Bonte, A., Colbeaux, J-P., Leplat, J., and Sommé, J., 1985, Boulogne-Sur-Mer: Bureau de Recherches Géologiques et Minières, Carte Géologique de la France à 1:50,000, Feuille 10.

Braaksma, H., Proust, J.N., Kenter, J.A.M., Drijkoningen, G.G., and Filippidou, N., 2006, Sedimentological, petrophysical, and seismic characterization of an Upper Jurassic shoreface-dominated shelf margin (the Boulonnais, northern France): Journal of Sedimentary Research, v. 76, p. 175-199.

Bradshaw, M.J., Cope, J.C.W., Cripps, D.W., Donovan, D.T., Howarth, M.K., Rawson, P.F., West, I.M., and Wimbledon, W.A., 1992, Jurassic, *in* Cope, J.C.W., Ingham, J.K., and Rawson, P.F., eds., Atlas of Palaeogeography and Lithofacies: Geological Society of London, Memoir 13, p. 107-129.

Bridge, J.S., and Best, J.L., 1988, Flow, sediment transport and bedform dynamics over the transition from dunes to upper-stage plane beds: implications for the formation of planar laminae: Sedimentology, v. 35, p. 753-763.

Bromley, R.G., and Ekdale, A.A., 1984, *Chondrites*: a trace fossil indicator of anoxia in sediments: Science, v. 224, p. 872-874.

Brookfield, M., 1973, Palaeogeography of the upper Oxfordian and lower Kimmeridgian (Jurassic) in Britain: Palaeogeography, Palaeoclimatology, Palaeoecology, v. 14, p. 137-167.

Butler, M., and Jamieson, R., 2013, Preliminary interpretation of six regional profiles across onshore basins of England: UK Onshore Geophysical Library. http://maps.lynxinfo.co.uk/docs/images/interpretations/

CANT, D.J., 1991, Geometric modelling of facies migration: theoretical development of facies successions and local unconformities: Basin Research, v. 3, p. 51-62.

CATTANEO, A. AND STEEL, R.J., 2003, Transgressive deposits: a review of their variability: Earth-Science Reviews, v. 62, p. 187-228.

CHADWICK, R.A., 1986, Extension tectonics in the Wessex Basin, southern England: Geological Society of London, Journal, v. 143, p. 465-488.

CHEEL, R.J., 1990, Horizontal lamination and the sequence of bed phases and stratification under upper-flow-regime conditions: Sedimentology, v. 37, p. 517-529.

CLIFTON, H.E., 1976, Wave-formed sedimentary structures — a conceptual model, *in* Davis, R.A., and Ethington, R.L., eds., Beach and Nearshore Processes: SEPM, Special Publication 24, p. 126-148.

CLIFTON, H.E., 2006, A re-examination of facies models for clastic shorelines, *in* Posamentier, H.W., and Walker, R.G., eds., Facies Models Revisited: SEPM, Special Publication 84, p. 293-337.

CLOUD JR., P.E., 1955. Physical limits of glauconite formation: American Association of Petroleum Geologists, Bulletin, v. 39, p. 484-492.

CUSHMAN-ROISIN, B., 1994, Introduction to Geophysical Fluid Dynamics: Prentice Hall, New Jersey, USA, 830 p.

DALRYMPLE, R.W., AND RHODES, R.N., 1995, Estuarine dunes and bars, *in* Perillo, G.M.E., ed., Geomorphology and Sedimentology of Estuaries: Amsterdam, Elsevier, Developments in Sedimentology, v. 53, p. 359-422..

DALRYMPLE, R.W., BAKER, E.K., HARRIS, P.T., AND HUGHES, M.G., 2003, Sedimentology and stratigraphy of a tide-dominated, foreland-basin delta (Fly River, Papua New Guinea), *in* Sidi, F.H., Nummedal, D., Imbert, P., Darman, H., and Posamentier, H.W., eds., Tropical Deltas of Southeast Asia — Sedimentology, Stratigraphy, and Petroleum Geology: SEPM, Special Publication 76, p. 147-173.

Dashtgard, S.E., Gingras, M.K., and MacEachern, J.A., 2009, Tidally modulated shorefaces: Journal of Sedimentary Research, v. 79, p. 793-807.

Dashtgard, S.E., MacEachern, J.A., Frey, S.E. and Gingras, M.K., 2012, Tidal effects on the shoreface: towards a conceptual framework: Sedimentary Geology, v. 279, p. 42-61.

Davidson-Arnott, R.G.D., and Greenwood, B., 1974, Bedforms and structures associated with bar topography in the shallow-water wave environment, Kouchibouguac Bay, New Brunswick, Canada: Journal of Sedimentary Petrology, v. 44, p. 698-704.

Davidson-Arnott, R.G.D., and Greenwood, B., 1976, Facies relations on a barred coast, Kouchibouguac Bay, New Brunswick, Canada, *in* Davis, R.A., and Ethington, R.L., eds., Beach and Nearshore Processes: SEPM, Special Publication 24, p. 149-168.

Dickinson, W.R., 1970, Interpreting detrital modes of graywacke and arkose: Journal of Sedimentary Petrology, v. 40, p. 695-707.

Dickinson, W.R., Beard, L.S., Brakenridge, G.R., Erjavec, J.L., Ferguson, R.C., Inman, K.F., Knepp, R.A., Lindberg, F.A., and Ryberg, P.T., 1983, Provenance of North American Phanerozoic sandstones in relation to tectonic setting: Geological Society of America, Bulletin, v. 94, p. 222-235.

Dott, R.H., and Bourgeois, J. 1982, Hummocky stratification: significance of its variable bedding sequences: Geological Society of America, Bulletin, v. 93, p. 663-680.

Duke, W.L., 1985, Hummocky cross stratification, tropical hurricanes, and intense winter storms: Sedimentology, v. 32, p. 167-194.

Dumas, S., Arnott, R.W.C., and Southard, J.B., 2005, Experiments on oscillatory-flow and combined-flow bed forms: implications for interpreting parts of the shallow-marine sedimentary record: Journal of Sedimentary Research, v. 75, p. 501-513.

Elliott, T., 1986, Clastic shorelines, *in:* Reading, H.G., ed., Sedimentary Environments and Facies: Blackwell Scientific Publications, Oxford, p. 143-177.

FISHER, R.V., 1971, Features of coarse-grained, high-concentration fluids and their deposits: Journal of Sedimentary Petrology, v. 41, p. 916-927.

FÖLLMI, K.B., 2016, Sedimentary condensation: Earth-Science Reviews, v. 152, p. 143-180.

FREY, S.E., AND DASHTGARD, S.E., 2011, Sedimentology, ichnology and hydrodynamics of strait-margin, sand and gravel beaches and shorefaces: Juan de Fuca Strait, British Columbia, Canada: Sedimentology, v. 58, p. 1326-1346.

FRUERGAARD, M., TESSIER, B., POIRIER, C., MOUAZÉ, D., WEILL, P., AND NOËL, S., 2020, Depositional controls on a hypertidal barrier-spit system architecture and evolution, Pointe du Banc spit, north-western France: Sedimentology, v. 67, p. 502-533.

FÜRSICH, F.T., 1986, Storm shell beds of *Nanogyra virgula* in the upper Jurassic of France: Neues Jahrbuch für Geologie Paläontologie, Abhandlungen, v. 172, p. 141-161.

GALEHOUSE, J.S., 1971, Point counting, *in:* Carver, R.E., ed., Procedures in Sedimentary Petrology: New York, Wiley-Interscience, p. 385-407.

GALLOIS, R., 2000, The stratigraphy of the Kimmeridge Clay Formation (Upper Jurassic) in the RGGE project boreholes at Swanworth Quarry and Metherhills, south Dorset: Proceedings of the Geologists' Association, v. 111, p. 265-280.

GAYNOR, G.C., AND SWIFT, D.J., 1988, Shannon Sandstone depositional model; sand ridge dynamics on the Campanian Western Interior Shelf: Journal of Sedimentary Petrology, v. 58, p. 868-880.

GEYSSANT, J.R., VIDIER, J.P., HERBIN, J.P., PROUST, J.N., AND DECONINCK, J.F., 1993. Biostratigraphie et paléoenvironnement des couches de passage Kimméridgien/Tithonien du Boulonnais (Pas-de-Calais): nouvelles données paléontologiques (ammonites), organisation séquentielle et contenu en matière organique: Géologie de la France, v. 4, p. 11-24.

GHADEER, S.G., AND MACQUAKER, J.H.S., 2011, Sediment transport processes in an ancient mud-dominated succession: a comparison of processes operating in marine offshore settings and anoxic basinal environments: Geological Society of London, Journal, v. 168, p. 1121-1132.

Gingras, M.K., MacEachern, J.A., and Dashtgard, S.E., 2011, Process ichnology and the elucidation of physico-chemical stress: Sedimentary Geology, v. 237, p. 115-134.

Hallam, A., 1984, Continental humid and arid zones during the Jurassic and Cretaceous: Palaeogeography, Palaeoclimatology, Palaeoecology, v. 47, p. 195-223.

Hampson, G.J., 2000, Discontinuity surfaces, clinoforms, and facies architecture in a wave-dominated, shoreface–shelf parasequence: Journal of Sedimentary Research, v. 70, p. 325-340.

Hampson, G.J., Rodriguez, A.B., Storms, J.E.A., Johnson, H.D., and Meyer, C.T., 2008, Architecture and genesis of intra-parasequence discontinuity surfaces in wave-dominated deltaic deposits: Upper Cretaceous Sunnyside Member, Blackhawk Formation, Book Cliffs, Utah, USA, *in* Hampson, G.J., Steel, R.J., Burgess, P.M., and Dalrymple, R.W., eds., Recent Advances in Models of Siliciclastic Shallow-Marine Stratigraphy: SEPM, Special Publication 90, p. 117-142.

Hansen, D.L., Blundell, D.J., and Nielsen, S.B., 2002, A model for the evolution of the Weald Basin: Geological Society of Denmark, Bulletin, v. 49, p. 109-118.

Hawkes, P.W., Fraser, A.J., and Einchcomb, C.C.G., 1998, The tectono-stratigraphic development and exploration history of the Weald and Wessex Basin, Southern England, UK, *in* Underhill, J.R., ed., Development, Evolution and Petroleum Geology of the Wessex Basin: Geological Society of London, Special Publication 133, p. 39-65.

Helland-Hansen, W. and Martinsen, O.J., 1996, Shoreline trajectories and sequences: description of variable depositional-dip scenarios: Journal of Sedimentary Research, v. B66, p. 670-688.

Hesselbo, S.P., Deconinck, J.F., Huggett, J.M., and Morgans-Bell, H.S., 2009, Late Jurassic palaeoclimatic change from clay mineralogy and gamma-ray spectrometry of the Kimmeridge Clay, Dorset, UK: Geological Society of London, Journal, v. 166, p. 1123-1133.

Hunter, R.E., Clifton, H.E., and Phillips, R.L., 1979, Depositional processes, sedimentary structures, and predicted vertical sequences in barred nearshore systems, southern Oregon coast: Journal of Sedimentary Petrology, v. 49, p. 711-726.

ICHASO, A.A., AND DALRYMPLE, R.W., 2009, Tide-and wave-generated fluid mud deposits in the Tilje Formation (Jurassic), offshore Norway: Geology, v. 37, p. 539-542.

ISLA, M.F., SCHWARZ, E., AND VEIGA, G.D., 2018, Bedset characterization within a wave-dominated shallow-marine succession: an evolutionary model related to sediment imbalances: Sedimentary Geology, v. 374, p. 36-52.

KANTOROWICZ, J.D, BRYANT, I.D., AND DAWANS, J.M., 1987, Controls on the geometry and distribution of carbonate cements in Jurassic sandstones: Bridport Sands, Southern England and Viking Group, Troll field, Norway, *in* Marshall, J.D., ed., Diagenesis of Sedimentary Sequences: Geological Society of London, Special Publication 36, p. 103-118.

KIDWELL, S.M., 1986, Models for fossil concentrations: paleobiologic implications: Paleobiology, v. 12, p. 6-24.

KRUMBLEIN, W.C. AND PETTIJOHN, F.J., 1938, Manual of Sedimentary Petrography: New York, Appleton-Century-Crofts, 549 p.

LAMB, M.P., AND PARSONS, J.D., 2005, High-density suspensions formed under waves: Journal of Sedimentary Research, v. 75, p. 386-397.

MACEACHERN, J.A., AND BANN, K.L., 2008, The role of ichnology in refining shallow marine facies models, *in* Hampson, G.J., Steel, R.J., Burgess, P.M., and Dalrymple, R.W., eds., Recent Advances in Models of Siliciclastic Shallow-Marine Stratigraphy: SEPM, Special Publication 90, p. 73-116.

MACEACHERN, J.A., RAYCHAUDHURI, I., AND PEMBERTON, S.G., 1992, Stratigraphic applications of the *Glossifungites* ichnofacies: delineating discontinuities in the rock record, *in* Pemberton, S.G., ed., Applications of Ichnology to Petroleum Exploration: SEPM, Core Workshop 17, p. 169-198.

MACQUAKER, J.H.S., AND GAWTHORPE, R.L., 1993, Mudstone lithofacies in the Kimmeridge Clay Formation, Wessex Basin, southern England: implications for the origin and controls of the distribution of mudstones: Journal of Sedimentary Petrology, v. 63, p. 1129-1143.

Mahieux, G., Proust, J.N., Tessier, B., and DeBatist, M., 1998, Comparison between high-resolution seismic and sequence stratigraphic approaches applied to the Upper Jurassic deposits of the Dover strait area (Northern France): Marine and Petroleum Geology, v. 15, p. 329-342.

Mansy, J.L., Manby, G.M., Averbuch, O., Everaerts, M., Bergerat, F., Van Vliet-Lanoë, B., Lamarche, J., and Vandycke, S., 2003, Dynamics and inversion of the Mesozoic Basin of the Weald–Boulonnais area: role of basement reactivation: Tectonophysics, v. 373, p. 161-179.

Mansy, J-L., Guennoc, P., Robaszynski, F., Amédro, F., Auffret, J-P., Vidier, J., Lamarche, J., Lefèvre, D., Sommé, J., Brice, D., Mistiaen, B., Prud'homme, A, Rohart, J.-C., and Vachard, D., 2007, Marquise: Bureau de Recherches Géologiques et Minières, Carte Géologique de la France à 1:50,000, Feuille 5.

Mitchell, A.J., Allison, P.A., Gorman, G.J., Piggott, M.D., and Pain, C.C., 2011, Tidal circulation in an ancient epicontinental sea: the Early Jurassic Laurasian Seaway: Geology, v. 39, p. 207-210.

Morris, J.E., Hampson, G.J., and Johnson, H.D., 2006, A sequence stratigraphic model for an intensely bioturbated shallow-marine sandstone: the Bridport Sand Formation, Wessex Basin, UK: Sedimentology, v. 53, p. 1229-1263.

Moslow, T.F., and Tye, R.S., 1985, Recognition and characterization of Holocene tidal inlet sequences: Marine Geology, v. 63, p. 129-151.

Nielsen, L.H., Johannessen, P.N., and Surlyk, F., 1988, A Late Pleistocene coarse-grained spit-platform sequence in northern Jylland, Denmark: Sedimentology, v. 35, p. 915-937.

Nummedal, D., and Swift, D.J.P., 1987, Transgressive stratigraphy at sequence-bounding unconformities: some principles derived from Holocene and Cretaceous example, *in* Nummedal, D., Pilkey, O.H., and Howard, S.D., eds., Sea Level Fluctuation and Coastal Evolution: SEPM, Special Publication 41, p. 241–260.

Ogg, J.G., and Hinnov, L.A., 2012, Jurassic, *in:* Gradstein, F.M., Ogg, J.G., Schmitz, M.D., and Ogg, G.M., eds., The Geologic Time Scale 2012: Amsterdam, Elsevier, p. 731-791.

Olariu, C., Steel, R.J., Dalrymple, R.W., and Gingras, M.K., 2012, Tidal dunes versus tidal bars: the sedimentological and architectural characteristics of compound dunes in a tidal seaway, the lower Baronia Sandstone (Lower Eocene), Ager Basin, Spain: Sedimentary Geology, v. 279, p. 134-155.

Paola, C., Heller, P.L., and Angevine, C.L., 1992, The large-scale dynamics of grain-size variation in alluvial basins, 1: theory: Basin Research, v. 4, p. 73-90.

Pearson, S.J., Marshall, J.E.A., and Kemp, A.E.S., 2004, The White Stone Band of the Kimmeridge Clay Formation, an integrated high-resolution approach to understanding environmental change: Geological Society of London, Journal, v. 161, p. 675-683.

Pemberton, S.G., and MacEachern, J.A., 1997, The ichnological signature of storm deposits: the use of trace fossils in event stratigraphy, *in* Brett, C.E., and Baird, G.C., eds., Paleontological Events: Stratigraphic, Ecological and Evolutionary Implications: Columbia University Press, New York, p. 73-109.

Pemberton, S.G., MacEachern, J.A., and Frey, R.W., 1992, Trace fossil facies models: environmental and allostratigraphic significance, *in* Walker, R.G., and James, N.P., eds., Facies Models; Response to Sea-Level Change: Geological Association of Canada, p. 47-72.

Pharaoh, T., 2018, The Anglo–Brabant Massif: persistent but enigmatic palaeo-relief at the heart of western Europe: Proceedings of the Geologists' Association, v. 129, p. 278-328.

Plint, A.G., 1988, Sharp-based shoreface sequences and "offshore bars" in the Cardium formation of Alberta: their relationship to relative changes in sea level, *in* Wilgus, C.K., Hastings, B.S., Kendall, C.G.St.C., Posamentier, H.W., Ross, C.A., and Van Wagoner, J.C., eds., Sea-Level Changes — An Integrated Approach: SEPM, Special Publication 42, p. 357-370.

Proust, J.N., Deconinck, J.F., Geyssant, J.R., Herbin, J.P., and Vidier, J.P., 1995, Sequence analytical approach to the Upper Kimmeridgian–Lower Tithonian storm-dominated ramp deposits of the Boulonnais (Northern France). A landward time-equivalent to offshore marine source rocks: Geologische Rundschau, v. 84, p. 255-271.

Proust, J.N., Mahieux, G., and Tessier, B., 2001, Field and seismic images of sharp-based shoreface deposits: Implications for sequence stratigraphic analysis: Journal of Sedimentary Research, v. 71, p. 944-957.

Pugh, D.T., 1987, Tides, Surges and Mean Sea-Level: a Handbook for Engineers and Scientists: London, John Wiley and Sons, 472 p.

Reineck, H.E., and Singh, I.B., 1973, Depositional Sedimentary Structures: Springer-Verlag, Berlin, 439 p.

Romans, B.W., Castelltort, S., Covault, J.A., Fildani, A., and Walsh, J.P., 2016, Environmental signal propagation in sedimentary systems across timescales: Earth-Science Reviews, v. 153, p. 7-29.

Rossi, V.M., Perillo, M.M., Steel, R.J., and Olariu, C., 2017, Quantifying mixed-process variability in shallow-marine depositional systems: What are sedimentary structures really telling us?: Journal of Sedimentary Research, v. 87, p. 1060-1074.

Savrda, C.E., and Bottjer, D.J., 1989: Trace-fossil model for reconstructing oxygenation histories of ancient marine bottom waters: application to Upper Cretaceous Niobrara Formation, Colorado: Palaeogeography, Palaeoclimatology, Palaeoecology, v. 74, p. 49-74.

Schlirf, M., 2003, Palaeoecologic significance of Late Jurassic trace fossils from the Boulonnais, N France: Acta Geologica Polonica, v. 53, p. 123-142.

Sellwood, B.W. and Valdes, P.J., 2008, Jurassic climates: Proceedings of the Geologists' Association, v. 119, p. 5-17.

Sixsmith, P.J., Hampson, G.J., Gupta, S., Johnson, H.D., and Fofana, J.J., 2008, Facies architecture of a net transgressive sandstone reservoir analog: the Cretaceous Hosta Tongue, New Mexico: American Association of Petroleum Geologists, Bulletin, v. , p. 513-547.

Southard, J.B., Lambie, J.M., Federico, D.C., Pile, H.T., and Weidman, C.R., 1990, Experiments on bed configurations in fine sand under bidirectional purely oscillatory flow, and the origin of hummocky cross stratification: Journal of Sedimentary Petrology, v. 60, p. 1-17.

Storms, J.E.A., and Hampson, G.J., 2005, Mechanisms for forming discontinuity surfaces within shoreface–shelf parasequences: sea level, sediment supply or wave regime?: Journal of Sedimentary Research, v. 75, p. 67-81.

Sun, S.Q., 1992, A storm-dominated offshore sandstone interval from the Corallian Group (Upper Jurassic), Weald Basin, southern England. Marine and Petroleum Geology, v. 9, p. 274-286.

Swift, D.J.P., 1968, Coastal erosion and transgressive stratigraphy: Journal of Geology, v. 76, p. 444–456.

Sztanò, O., and De Boer, P.L., 1995, Basin dimensions and morphology as controls on amplification of tidal motions (the Early Miocene North Hungarian Bay): Sedimentology, v. 42, p. 665-682.

Sømme, T.O., Howell, J.A., Hampson, G.J., and Storms, J.E.A., 2008, Architecture and genesis of intra-parasequence discontinuity surfaces in wave-dominated deltaic deposits: Upper Cretaceous Sunnyside Member, Blackhawk Formation, Book Cliffs, Utah, USA, *in* Hampson, G.J., Steel, R.J., Burgess, P.M., and Dalrymple, R.W., eds., Recent Advances in Models of Siliciclastic Shallow-Marine Stratigraphy: SEPM, Special Publication 90, p. 421-441.

Tanner, W.F., 1960, Shallow water ripple mark varieties: Journal of Sedimentary Petrology, v. 30, p. 481-485.

Taylor, A.M., and Goldring, R., 1993, Description and analysis of bioturbation and ichnofabric: Geological Society of London, Journal, v. 150, p. 141-148.

Taylor, S.P., and Sellwood, B.W., 2002, The context of lowstand events in the Kimmeridgian (Late Jurassic) sequence stratigraphic evolution of the Wessex–Weald Basin, Southern England: Sedimentary Geology, v. 151, p. 89-106.

Taylor, S.P., Sellwood, B.W., Gallois, R.W., and Chambers, M.H., 2001, A sequence stratigraphy of the Kimmeridgian and Bolonian stages (late Jurassic): Wessex–Weald Basin, southern England: Geological Society of London, Journal, v. 158, p. 179-192.

Traykovski, P., Geyer, W.R., Irish, J.D., and Lynch, J.F., 2000, The role of wave-induced density-driven fluid mud flows for cross-shelf transport on the Eel River continental shelf: Continental Shelf Research, v. 20, p. 2113–2140.

Trueman, S., 2003, The Humbly Grove, Herriard, Storrington, Singleton, Stockbridge, Goodworth, Horndean, Palmers Wood, Bletchingley and Albury fields, Hampshire, Surrey and Sussex, UK onshore, *in* Gluyas, J.G., and Hitchens, H.M., eds., United Kingdom Oil and Gas Fields, Commemorative Volume: Geological Society of London, Memoir 20, p. 929-941.

Tyson, R.V., Wilson, R.C.L., and Downie, C., 1979, A stratified water column environmental model for the type Kimmeridge Clay: Nature, v. 277, p. 377-380.

Vakarelov, B.K., Ainsworth, R.B., and MacEachern, J.A., 2012, Recognition of wave-dominated, tide-influenced shoreline systems in the rock record: variations from a microtidal shoreline model: Sedimentary Geology, v. 279, p. 23-41.

Vaucher, R., Pittet, B., Hormière, H., Martin, E.L. and Lefebvre, B., 2017, A wave-dominated, tide-modulated model for the Lower Ordovician of the Anti-Atlas, Morocco: Sedimentology, v. 64, p. 777-807.

Vaucher, R., Pittet, B., Passot, S., Grandjean, P., Humbert, T., and Allemand, P., 2018, Bedforms in a tidally modulated ridge and runnel shoreface (Berck-Plage; North France): implications for the geological record: Société Géologique de France, Bulletin, v. 189 (5), 15 p.

Wignall, P.B., 1989, Sedimentary dynamics of the Kimmeridge Clay: tempests and earthquakes: Geological Society of London, Journal, v. 146, p. 273-284.

Wignall, P.B., 1990, Ostracod and foraminifera micropaleoecology and its bearing on biostratigraphy: a case study from the Kimmeridgian (Late Jurassic) of North West Europe: Palaios, v. 5, p.219-226.

Wignall, P.B., 1991, Test of the concepts of sequence stratigraphy in the Kimmeridgian (Late Jurassic) of England and northern France: Marine and Petroleum Geology, v. 8, p. 430-441.

WIGNALL, P.B., AND RUFFELL, A.H., 1990, The influence of a sudden climatic change on marine deposition in the Kimmeridgian of northwest Europe: Geological Society of London, Journal, v. 147, p. 365-371.

WIGNALL, P.B., SUTCLIFFE, O.E., CLEMSON, J., AND YOUNG, E., 1996, Unusual shoreface sedimentology in the Upper Jurassic of the Boulonnais, northern France: Journal of Sedimentary Research, v. *66*, p. 577-586.

WILLIAMS, C.J., HESSELBO, S.P., JENKYNS, H.C. AND MORGANS-BELL, H.S., 2001, Quartz silt in mudrocks as a key to sequence stratigraphy (Kimmeridge Clay Formation, Late Jurassic, Wessex Basin, UK): Terra Nova, v. 13, p. 449-455.

YOSHIDA, S., STEEL, R.J., AND DALRYMPLE, R.W., 2007, Changes in depositional processes—an ingredient in a new generation of sequence-stratigraphic models: Journal of Sedimentary Research, v. 77, p. 447-460.

ZIEGLER, P.A., 1989, Evolution of the North Atlantic—an overview, *in* Tankard, A.J., and Balkwill, H.R., eds., Extensional Tectonics and Stratigraphy of the North Atlantic Margins: American Association of Petroleum Geologists, Memoir 46, p. 111-129.

FIGURE CAPTIONS

Figure 1

A) Regional Late Jurassic paleogeographic setting of the transcontinental Laurasian Seaway of northwestern Europe, which connected the Tethys Ocean to the southeast with the incipient Atlantic Ocean to the northwest (after Ziegler 1989; Hesselbo et al. 2009). **B**) Late Jurassic paleogeography of the Weald Basin, southern UK, its extension in the Boulonnais region, northern France, and surrounding areas (after Bradshaw et al. 1992; Proust et al. 1995; Wignall et al. 1996). The study area (Fig. 2) is highlighted. **C**) Lithostratigraphy, biostratigraphy, and sequence stratigraphy of Kimmeridgian–Tithonian strata in the Weald Basin and Boulonnais region. Ammonite zonal boundaries are from Geyssant et al. (1993), Proust et al. (1995), and Braaksma et al. (2006) in Boulonnais, and from Taylor et al. (2001) and Taylor and Sellwood (2002) in the Weald Basin. Absolute ages for selected international stage boundaries and Boreal ammonite zonal boundaries are taken from Ogg and Hinnov (2012) (their Figure 26.8). The sequence stratigraphic framework for the Weald Basin of Taylor et al. (2001) and Taylor and Sellwood (2002) is shown. This framework is used as the basis for the nomenclature of sequence stratigraphic surfaces interpreted in this study, which are annotated on lithostratigraphic columns of the Weald Basin and the Boulonnais region.

Figure 2

Map showing the surface geology of the Weald Basin, southern UK, and its extension in the Boulonnais region, northern France. Well and outcrop data used in this study are shown. Abbreviated names of key wells: A1, Ashour 1; As2, Ashdown 2; Ba1, Balcombe 1; Br1, Brightling 1; D1, Detention 1; F1, Fairlight 1; GB1, Godley Bridge 1; H1, Holtye 1; IG1, Iden Green 1; LK1A, Lower Kingswood 1A; PW1-5, Palmers Wood 1-5; R1, Rotherfield 1; TH1, Turners Hill 1; W1, Wallcrouch 1. Abbreviated names of outcrop locations: CdlC, Cap de la Crèche; CGN, Cap Gris Nez; CP, Cran Poulet; LP, Le Portel; PdNdC, Pointe du Nid de Corbet.

Figure 3

Photograph of the Grès de Châtillon, Argiles de Châtillon, and lower and upper Grès de la Crèche (Fig. 1B) exposed directly south of Cap de la Crèche (Fig. 2). Upward-coarsening and upward-fining grain-size trends in the Grès de Châtillon and Grès de la Crèche are indicated respectively by upward-widening and upward-narrowing triangles.

Figure 4

Measured sections illustrating facies associations and facies successions in Kimmeridgian–Tithonian sandstones at outcrops in the Boulonnais region: **A**) Grès de Châtillon at Cran Poulet, **B**) Grès de Châtillon at Pointe du Nid de Corbet, **C**) Grès de la Crèche at Cap Gris Nez, and **D**) Grès de la Crèche at Le Portel. Outcrops are located in Figure 2, and the stratigraphic position of the exposed sandstones is shown in Figures 1B and 3. The lower and upper Grès de la Crèche are labelled in Figure 4C and D, based on the seismic and outcrop mapping of Proust et al. (2001; their Figure 6). Petrographic sample locations (Fig. 14) are indicated with an asterisk.

Figure 5

Measured sections illustrating facies associations and facies successions in cores through Kimmeridgian–Tithonian sandstones at **A**) Palmers Wood 3, **B**) Palmers Wood 2, **C**) Palmers Wood 5, **D**) Palmers Wood 4 (core 3), **E**) Holtye 1, **F**) Ashour 1, **G**) Rotherfield 1, **H**) Fairlight 1, and **I**) Iden Green 1. Cored wells are located in Figure 2, and the stratigraphic position of the cored intervals is shown in Figures 1B and 12. Petrographic sample locations (Fig. 14) are indicated with an asterisk. Key as for Figure 4.

Figure 6

Photographs illustrating characteristics of Facies Association 1 in core. **A**) Pale-colored, nodular, calcareous claystones intercalated with dark-colored, silty claystones. Bioturbation comprises *Chondrites* (*Ch*) and *Thalassinoides* (*Th*) (732.1 m in Rotherfield 1; Fig. 5G). **B**) Bioturbated siltstone containing *Chondrites* (*Ch*), *Planolites* (*Pl*), and *Zoophycos* (*Z*) (730.3 m in Rotherfield 1; Fig. 5G). **C**) Bioturbated sandy siltstone containing *Chondrites* (*Ch*), *Planolites* (*Pl*), *Palaeophycus* (*Pa*), *Teichichnus* (*T*), and *Zoophycos* (*Z*) (1097.3 m in Palmers Wood 3; Fig. 5A). **D**) Bioturbated siltstone with disarticulated and fragmented, thin bivalve shells (472.7 m in Iden Green 1; Fig. 5I). Coin of 2 cm diameter for scale.

Figure 7

Photographs illustrating characteristics of Facies Association 2 at outcrop and in core. **A–C**) Bioturbated sandstone beds and siltstone interbeds containing *Chondrites* (*Ch*), *Planolites* (*Pl*), *Palaeophycus* (*Pa*), *Teichichnus* (*T*), *Zoophycos* (*Z*), and *Thalassinoides* (*Th*) (954.5 m and 953.0 m in Holtye 1; Fig. 5E and 727.3 m in Rotherfield 1; Fig. 5G). Coin of 2 cm diameter for scale. **D**) Bioturbated sandy siltstone interbed between sandstone beds. Bioturbation comprises *Chondrites* (*Ch*), *Planolites* (*Pl*), *Palaeophycus* (*Pa*), and *Thalassinoides* (*Th*) (1094.5 m in Palmers Wood 3; Fig. 5A). **E**) Charcoal fragment in bioturbated sandstone bed (8.0 m in Cap Gris Nez log; Fig. 4C). Finger for scale. **F**) Low-angle cross-lamination in sandstone bed (30.4 m in Cap Gris Nez log; Fig. 4C). Pen for scale. **G**) Intensely bioturbated sandstone beds containing prominent *Rhizocorallium* (*Rh*) and *Thalassinoides* (*Th*) (1.2 m in Cran Poulet log; Fig. 4A).

Figure 8

Photographs illustrating characteristics of Facies Association 3 at outcrop and in core. **A**) Mudclasts and *Ophiomorpha* (*O*) in cross-bedded sandstone (980.0 m in Holtye 1; Fig. 5E). **B**) Sparsely bioturbated mudstones in between sandstone cross-sets. Bioturbation comprises *Planolites* (*Pl*) and *Thalassinoides* (*Th*) (978 m in Holtye 1; Fig. 5E). **C**) Cross-bedded sandstone (13.0 m in Cap Gris Nez log; Fig. 3C). **D**) Charcoal lining toesets of sandstone cross-set (4.3 m in Pointe du Nid de Corbet log; Fig. 4B). **E–G**) Cross-bedded sandstone in which symmetrical ripples overprint trough-shaped erosion surfaces. Rippled surfaces contain mudclasts and *Ophiomorpha* (*O*), and are draped by discontinuous mudstones (labelled “m” in Part E) (0–3.0 m in Pointe du Nid de Corbet log; Fig. 4B). **H**) Symmetrical ladder ripples on bedding plane (0–3.0 m in Pointe du Nid de Corbet log; Fig. 4B). **I**) Pervasive mottled fabric in sandstone due to overprinting by roots; individual root traces are picked out where distinct (r) (18.8 m in Cap Gris Nez log; Fig. 4C). Coin of 2 cm diameter (Fig. 8A, B), finger (Fig. 8D), compass-clinometer (Fig. 8F), and pen (Fig. 8G, H) for scale.

Figure 9

Photographs illustrating characteristics of Facies Association 4 at outcrop and in core. **A**) Bioclastic lag containing disarticulated and fragmented, thin bivalve shells (465.7 m in Iden Green 1; Fig. 5I). **B**) Bioclastic lag containing abraded, disarticulated, thick bivalve shells (1089.9 m in Palmers Wood 3; Fig. 5A). **C**, **D**) Bioclastic lag containing charcoal fragments and disarticulated, thin bivalve shells. The lag overlies a surface marked by *Thalassinoides* (*Th*) filled by coarse-grained, bioclastic sandstone that extend into underlying medium-grained sandstone (4.9 m in Pointe du Nid de Corbet log; Fig. 4B). **E**) Bioclastic lag containing extrabasinal pebbles of quartz and reworked sandstone, seen in bedding-plane view (2.0 m in Le Portel log; Fig. 4B). Coin of 2 cm diameter (Fig. 9A), finger (Fig. 9C), and pens (Fig. 9D, E) for scale.

Figure 10

A–C) Uninterpreted sparker profiles (upper) and geoseismic interpretations (lower), and **D**) paleogeographic map (cf. Fig. 1B) locating sparker profiles in the area offshore of the present-day Boulonnais outcrops, northern France (Fig. 2). **A**) Depositional-dip-oriented profile Bdb93005 through the Grès de Châtillon (after Figure 3 in Mahieux et al. 1998; Figure 8 in Proust et al. 2001); **B**) depositional-dip-oriented part of profile Bdb93028 through the Grès de la Crèche (after Figure 9B in Proust et al. 2001); and **C**) depositional-strike-oriented profile Bdb95004 through the Grès de la Crèche (after Figure 11C in Braaksma et al. 2006). The lower and upper Grès de la Crèche are labelled in Parts B and C, based on the seismic and outcrop mapping of Proust et al. (2001; their Figure 6).

Figure 11

A) Correlation panel between measured sections in the Boulonnais outcrops (modified from Proust et al. 2001). The outcrop belt is folded and faulted (Bonte et al. 1985; Mansy et al. 2007), and shallow, high-resolution seismic data (e.g., Fig. 10) has been used to aid correlation (Mahieux et al. 1998; Proust et al. 2001). The panel is oriented north–south. **B**) Northerly and **C**) southerly well correlation panels oriented west–east across the Weald Basin. Correlations are based on gamma-ray log patterns calibrated to lithology data from cores and cuttings, and are consistent with previous well correlations (Taylor et al. 2001; Taylor and Sellwood 2002). Regressive–transgressive tongues and their bounding flooding surfaces have been correlated, and the latter named according to the stratigraphic nomenclature of Taylor et al. (2001) and Taylor and Sellwood (2002). Correlation panels are located in Figure 2.

Figure 12

Facies model for Kimmeridgian–Tithonian sandstones in the Weald Basin, southern UK and Boulonnais region, northern France, as the deposits of high-energy, tidally modulated, barred shorefaces developed under conditions of high fairweather-wave energy and low storm-wave energy (after Davidson-Arnott and Greenwood 1976, Hunter et al. 1979, Wignall et al. 1996, Dashtgard et al. 2012). The model portrays **A**) shoreface progradation directed offshore and locally alongshore around a spit (cf. Nielsen et al. 1988; Fruergaard et al. 2020), under either **B**) an ascending regressive shoreline trajectory, with a discontinuous erosion surface formed at the base of the upper shoreface by bar migration (dashed red line), or **C**) a descending regressive shoreline trajectory, leading to enhanced erosion at the base of the upper shoreface (solid red line). Evidence of subaerial exposure is inferred to have been removed by subsequent transgressive erosion for both regressive trajectories.

Figure 13

Maps showing the distribution of regressive–transgressive sandstone tongues (Figs. 1, 11) at their maximum regressive extent, from oldest to youngest: **A**) beneath Km3 flooding surface, **B**) beneath Km6.1 flooding surface, **C**) beneath Km6.2 flooding surface (Grès de Connincthun), **D**) beneath Km6.3

flooding surface, **E**) beneath Km6.5 flooding surface (Grès de Châtillon), **F**) beneath Km7 flooding surface, and **G**) beneath Km7.5 flooding surface (Grès de la Crèche).

Figure 14

A) Ternary diagram showing the petrographic composition of Kimmeridgian–Tithonian sandstones from the subsurface Weald Basin and Boulonnais outcrops. Sandstones occur in the quartzose recycled-orogen field (cf. Dickinson et al. 1983). **B–D**) Thin-section photomicrographs of representative sandstone textures under plane-polarized light: **B**) medium-grained, cross-bedded sandstones of Facies Association 3 (3.2 m in Pointe du Nid de Corbet log; Fig. 4B); **C**) bioturbated silty sandstones of Facies Association 2 (606.2 m in Fairlight 1; Fig. 5H); and **D**) medium- to coarse-grained, cross-bedded sandstones of Facies Association 3 (973.0 m in Holtye 1; Fig. 5E). Monocrystalline quartz (m) is the most abundant detrital component of all samples, which also contain glauconite grains (gl), bioclasts (bi), grain-lining clays (cl), and poikilotopic calcite cement (po).

Figure 15

Summary of inferred controls on wave (red) and tide (blue) influence on late Jurassic shorelines along the northeastern margin of the Weald Basin. **A**) Prevailing westerly and southwesterly wind directions associated with Hadley-cell circulation imply a wave fetch of 200–600 m, while tidal wave propagated into the Laurasian Seaway from the Tethys Ocean. **B**) Constriction of the tidal wave in narrow (220 km wide) straits at the southeastern entrance to the Weald Basin elevated bed shear stress due to tidal currents, while semidiurnal tides were amplified by resonance in the shallow (18–33 m), wide (150–200 km), open embayment of the Weald Basin.

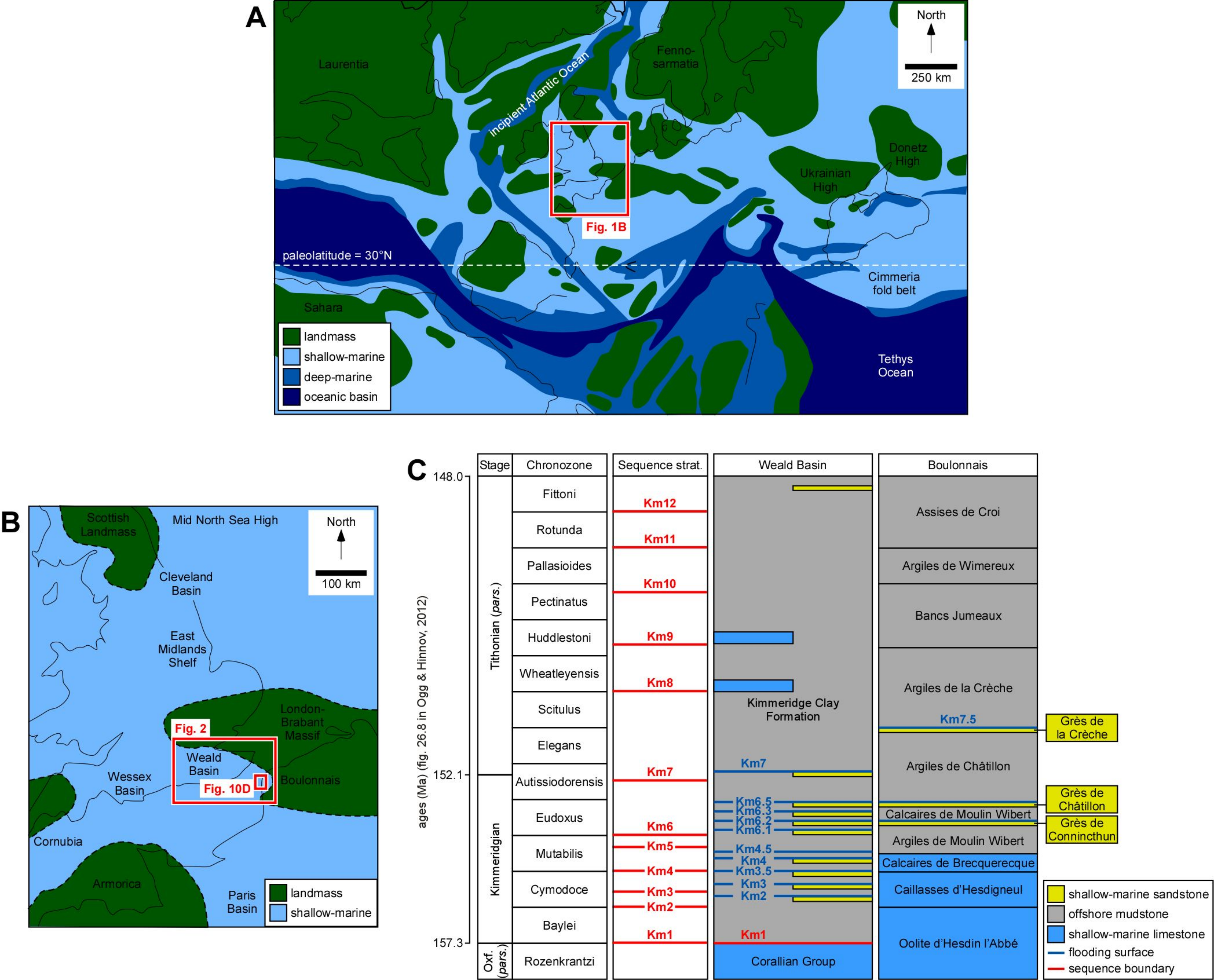

A
North
250 km
Laurentia
Fenno-
sarmatia
incipient Atlantic Ocean
Fig. 1B
Donetz
High
Ukrainian
High
paleolatitude = 30°N
Cimmeria
fold belt
Sahara
Tethys
Ocean
landmass
shallow-marine
deep-marine
oceanic basin
B
Scottish
Landmass
Mid North Sea High
North
100 km
Cleveland
Basin
East
Midlands
Shelf
London-
Brabant
Massif
Fig. 2
Weald
Basin
Wessex
Basin
Fig. 10D
Boulonnais
Cornubia
Armorica
Paris
Basin
landmass
shallow-marine
C
Stage
Chronozone
Sequence strat.
Weald Basin
Boulonnais
ages (Ma) (fig. 26.8 in Ogg & Hinnov, 2012)
148.0
152.1
157.3
Tithonian (pars.)
Kimmeridgian
Oxf. (pars.)
Fittoni
Rotunda
Pallasioides
Pectinatus
Huddlestoni
Wheatleyensis
Scitulus
Elegans
Autissiodorensis
Eudoxus
Mutabilis
Cymodoce
Baylei
Rozenkrantzi
Km12
Km11
Km10
Km9
Km8
Km7
Km6
Km5
Km4
Km3
Km2
Km1
Kimmeridge Clay
Formation
Km7
Km6.5
Km6.3
Km6.2
Km6.1
Km4.5
Km4
Km3.5
Km3
Km2
Km1
Corallian Group
Assises de Croi
Argiles de Wimereux
Bancs Jumeaux
Argiles de la Crèche
Km7.5
Argiles de Châtillon
Calcaires de Moulin Wibert
Argiles de Moulin Wibert
Calcaires de Brecquerecque
Caillasses d'Hesdigneul
Oolite d'Hesdin l'Abbé
Grès de
la Crèche
Grès de
Châtillon
Grès de
Connincthun
shallow-marine sandstone
offshore mudstone
shallow-marine limestone
flooding surface
sequence boundary

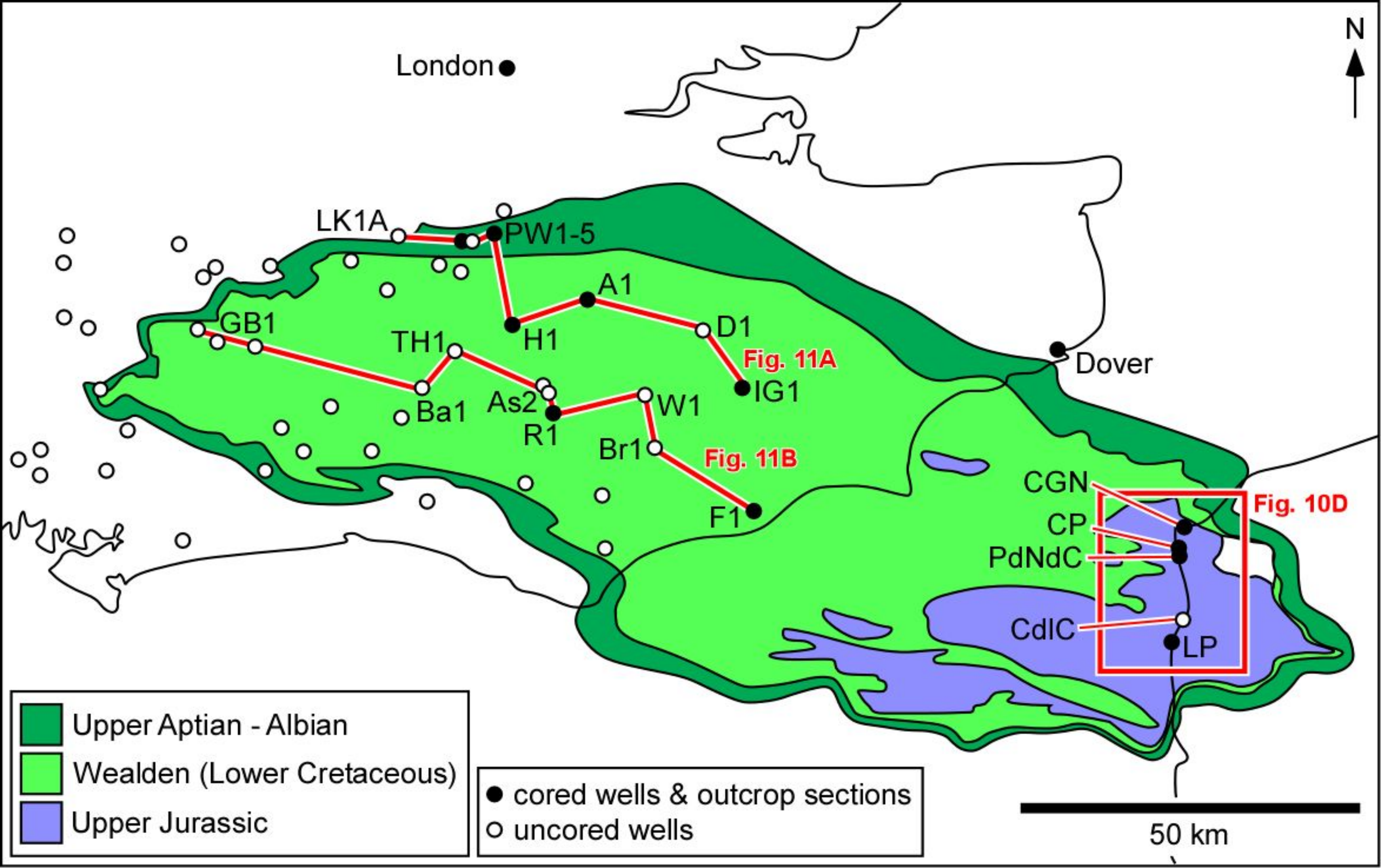

N
London
LK1A
PW1-5
A1
GB1
TH1
H1
D1
Fig. 11A
Dover
IG1
As2
W1
Ba1
R1
Br1
Fig. 11B
CGN
Fig. 10D
CP
F1
PdNdC
CdlC
LP
Upper Aptian - Albian
Wealden (Lower Cretaceous)
Upper Jurassic
cored wells & outcrop sections
uncored wells
50 km

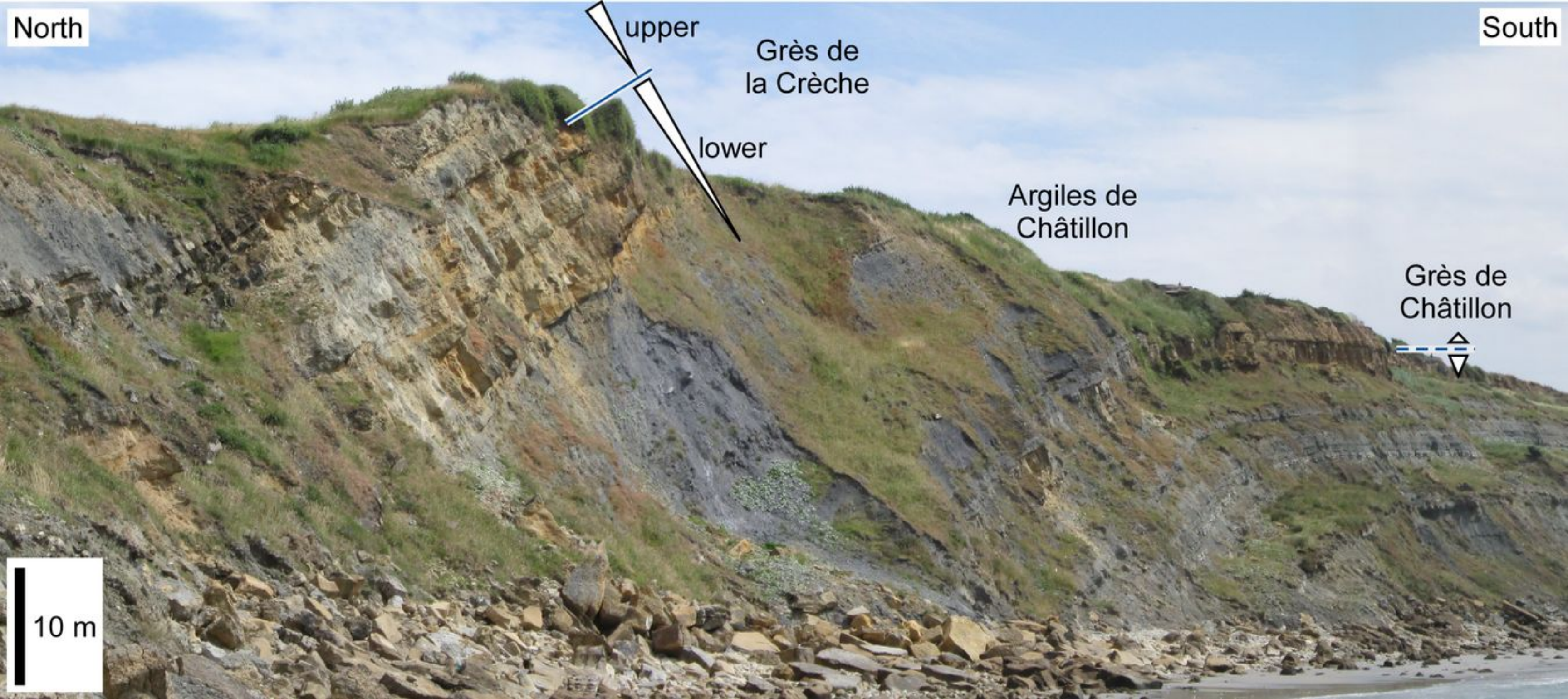
North
South
upper
lower
Grès de
la Crèche
Argiles de
Châtillon
Grès de
Châtillon
10 m

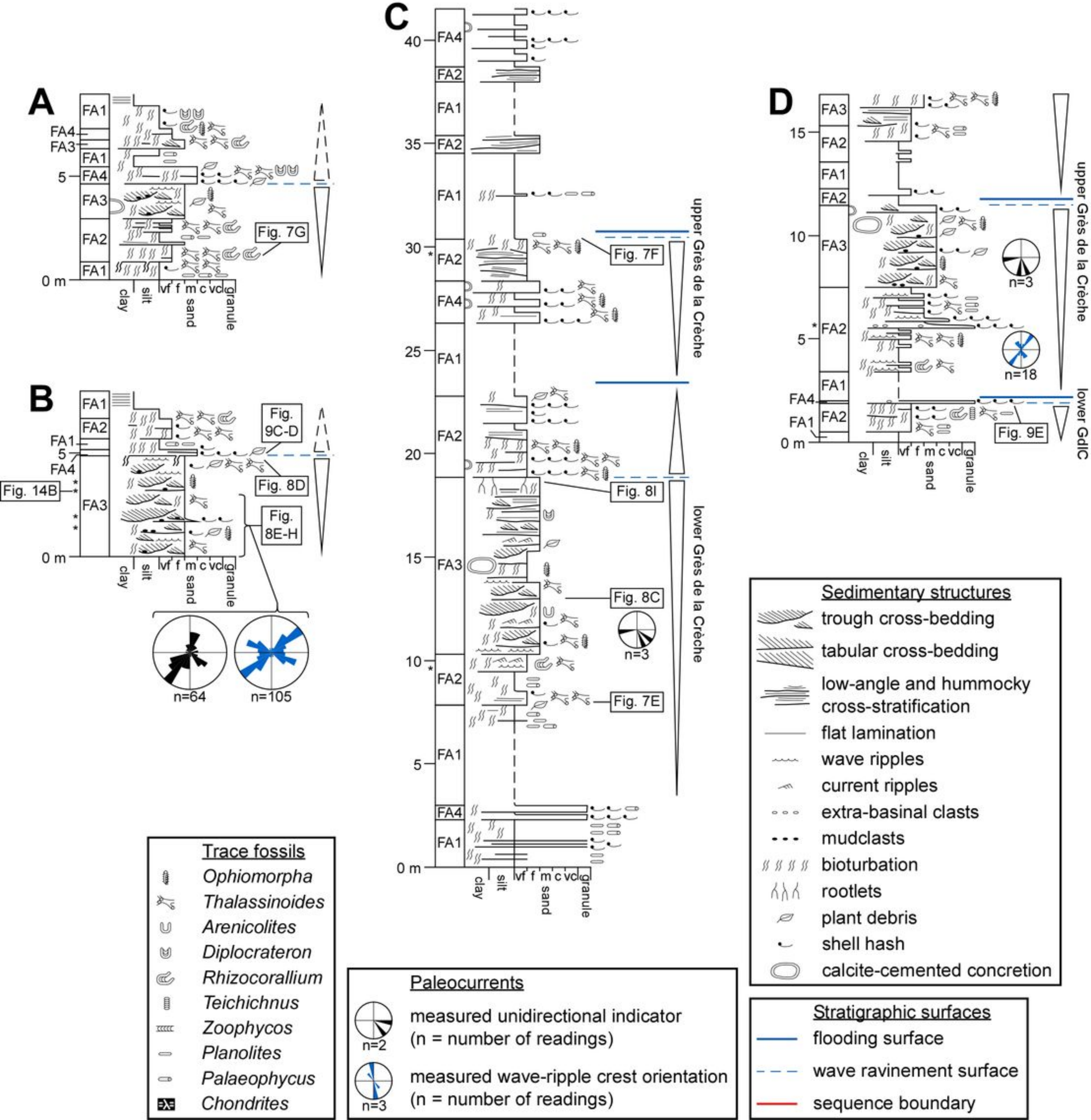
A
B
C
D
FA1
FA2
FA3
FA4
0 m
5
10
15
20
25
30
35
40
clay
silt
vf
f
m
c
vc
sand
granule
Fig. 7G
Fig. 9C-D
Fig. 8D
Fig. 14B
Fig. 8E-H
Fig. 7F
Fig. 8I
Fig. 8C
Fig. 7E
Fig. 9E
n=64
n=105
n=3
n=18
upper Grès de la Crèche
lower Grès de la Crèche
lower GdlC
Trace fossils
Ophiomorpha
Thalassinoides
Arenicolites
Diplocrateron
Rhizocorallium
Teichichnus
Zoophycos
Planolites
Palaeophycus
Chondrites
Paleocurrents
measured unidirectional indicator (n = number of readings)
n=2
measured wave-ripple crest orientation (n = number of readings)
n=3
Sedimentary structures
trough cross-bedding
tabular cross-bedding
low-angle and hummocky cross-stratification
flat lamination
wave ripples
current ripples
extra-basinal clasts
mudclasts
bioturbation
rootlets
plant debris
shell hash
calcite-cemented concretion
Stratigraphic surfaces
flooding surface
wave ravinement surface
sequence boundary

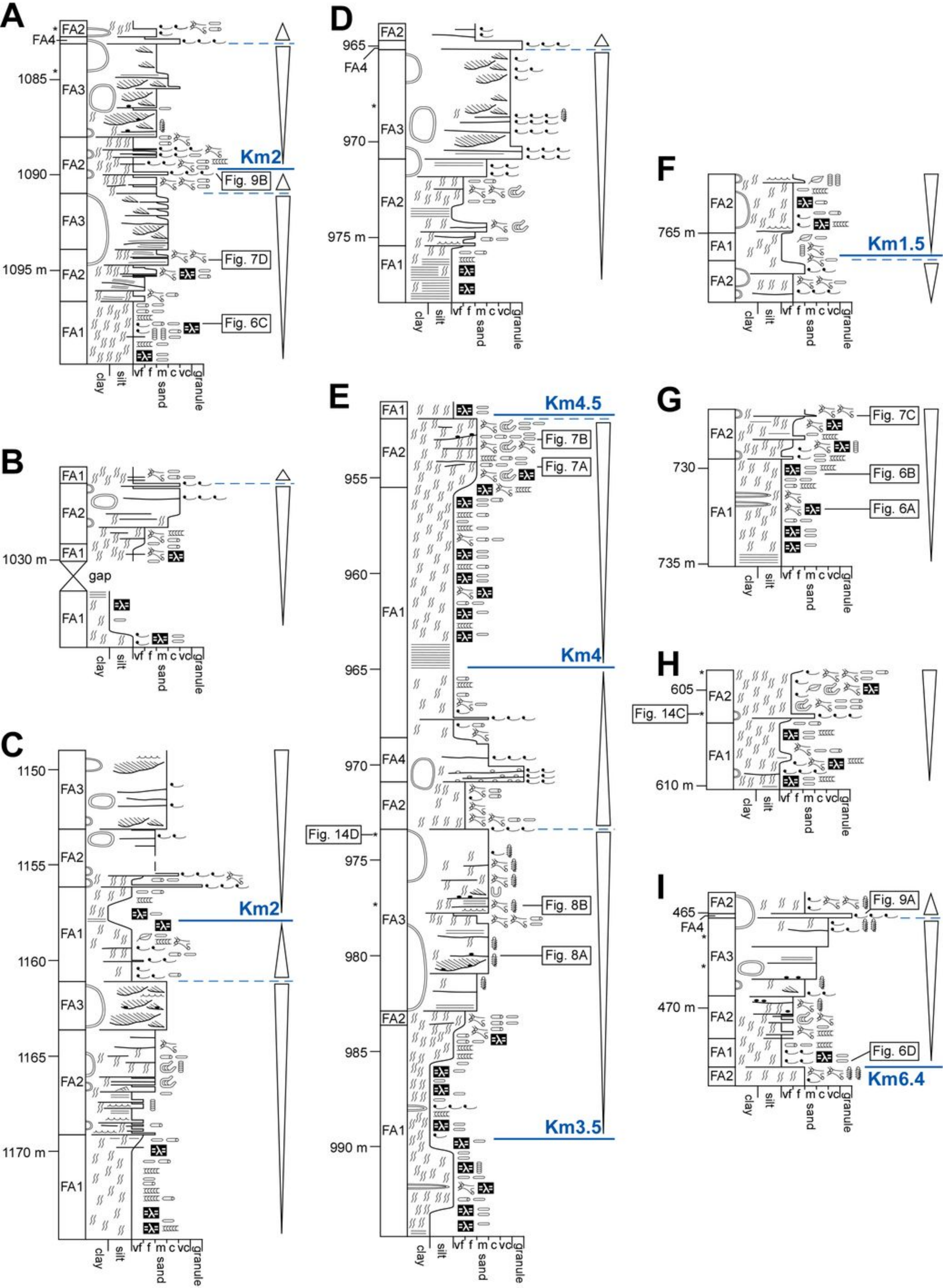

A
B
C
D
E
F
G
H
I
FA1
FA2
FA3
FA4
Km1.5
Km2
Km3.5
Km4
Km4.5
Km6.4
Fig. 6A
Fig. 6B
Fig. 6C
Fig. 6D
Fig. 7A
Fig. 7B
Fig. 7C
Fig. 7D
Fig. 8A
Fig. 8B
Fig. 9A
Fig. 9B
Fig. 14C
Fig. 14D
gap
1085
1090
1095 m
1030 m
1150
1155
1160
1165
1170 m
965
970
975 m
955
960
975
980
985
990 m
765 m
730
735 m
605
610 m
465
470 m
clay
silt
vf
f
m
c
vc
sand
granule

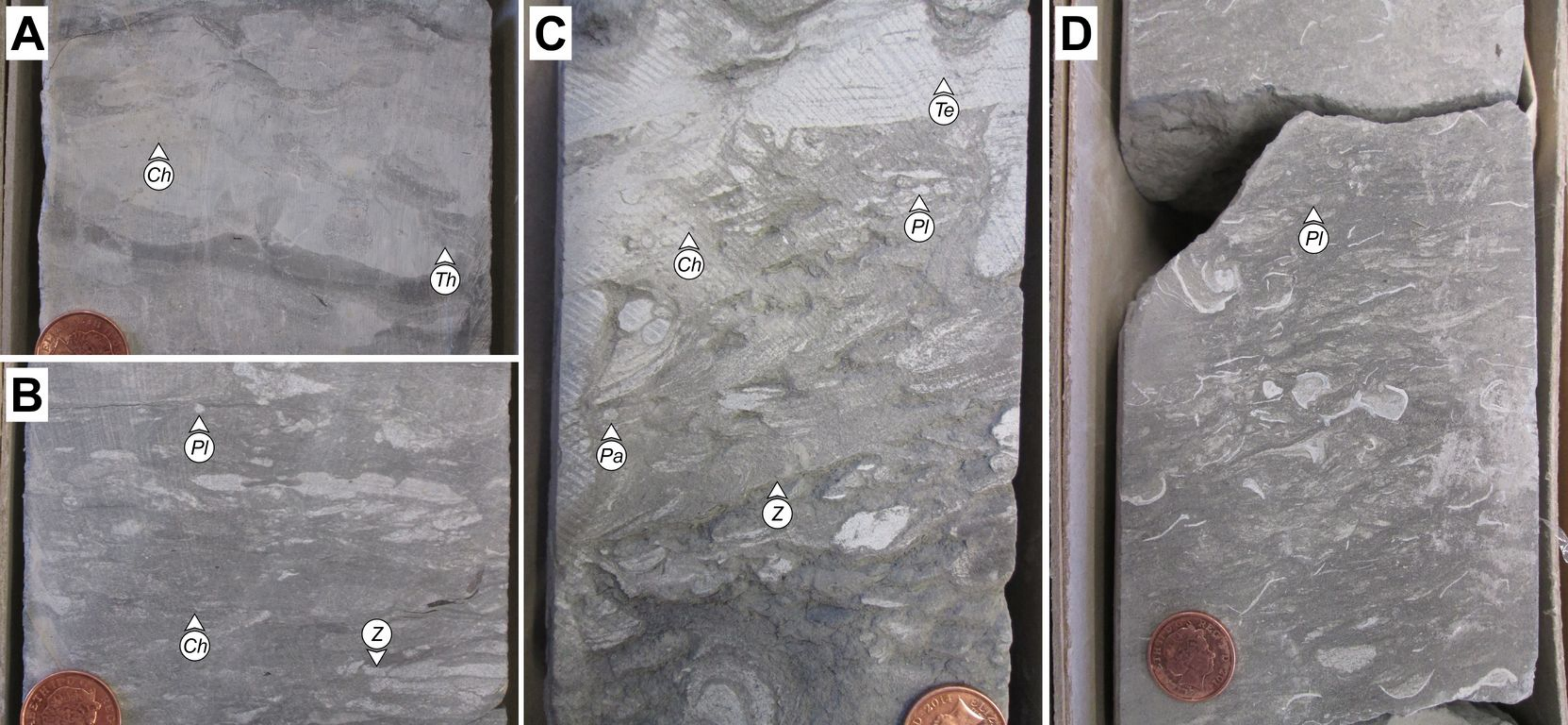
A
Ch
Th
B
Pl
Ch
Z
C
Te
Pl
Ch
Pa
Z
D
Pl

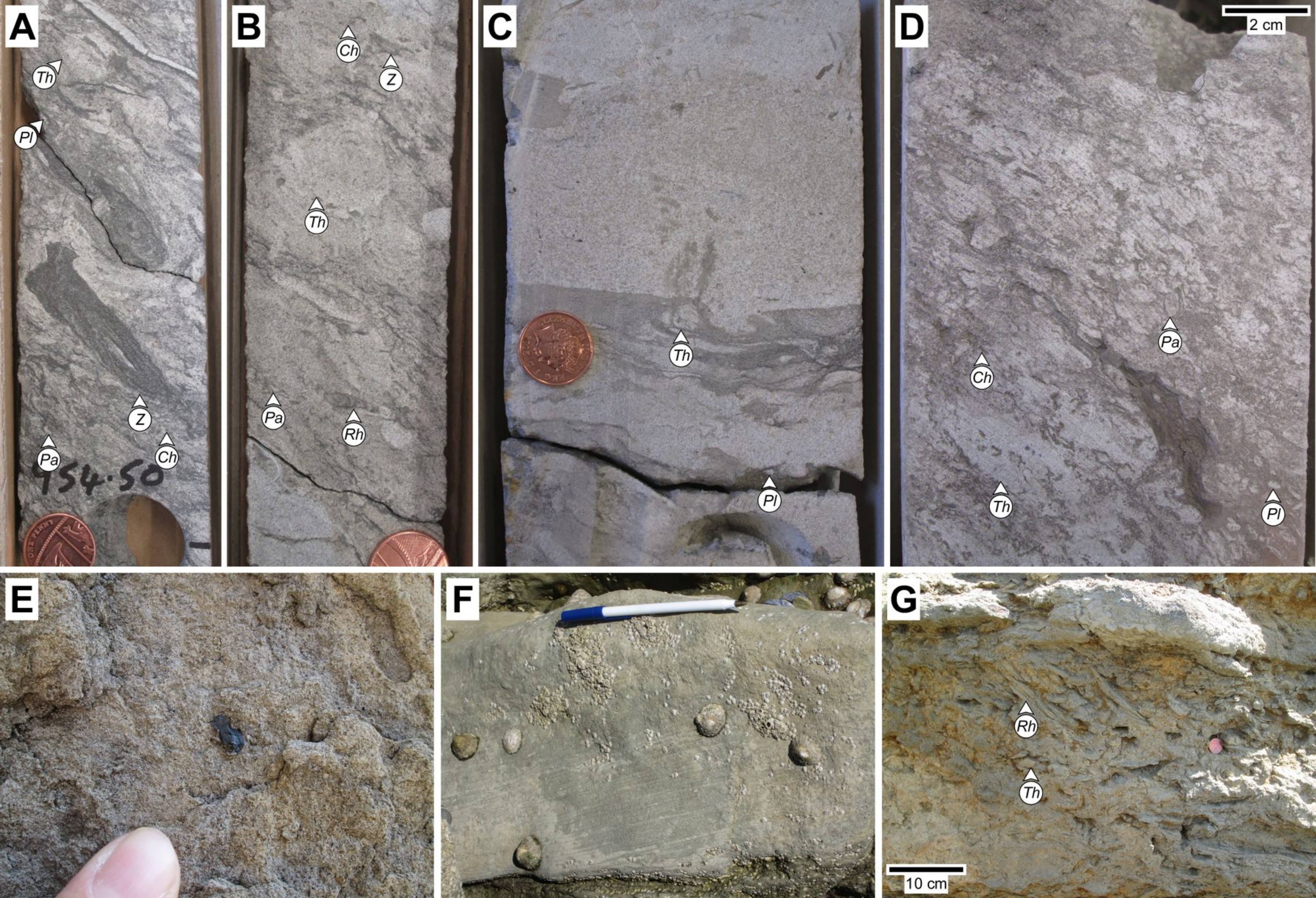
A
Th
Pl
Z
Pa
Ch
954·50
B
Ch
Z
Th
Pa
Rh
C
Th
Pl
D
2 cm
Pa
Ch
Th
Pl
E
F
G
Rh
Th
10 cm

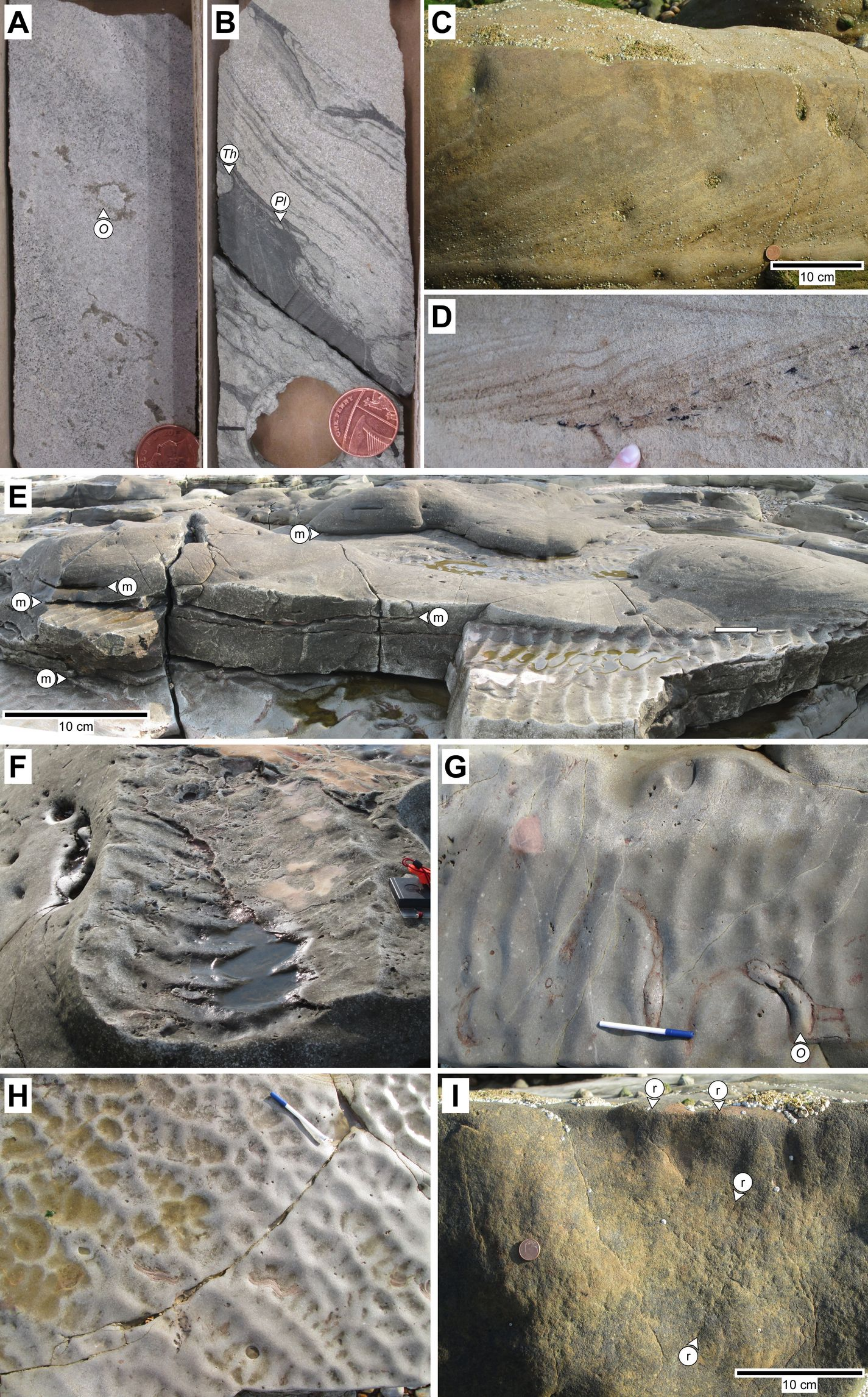

A
O
B
Th
Pl
C
10 cm
D
E
m
m
m
m
m
10 cm
F
G
O
H
I
r
r
r
r
10 cm

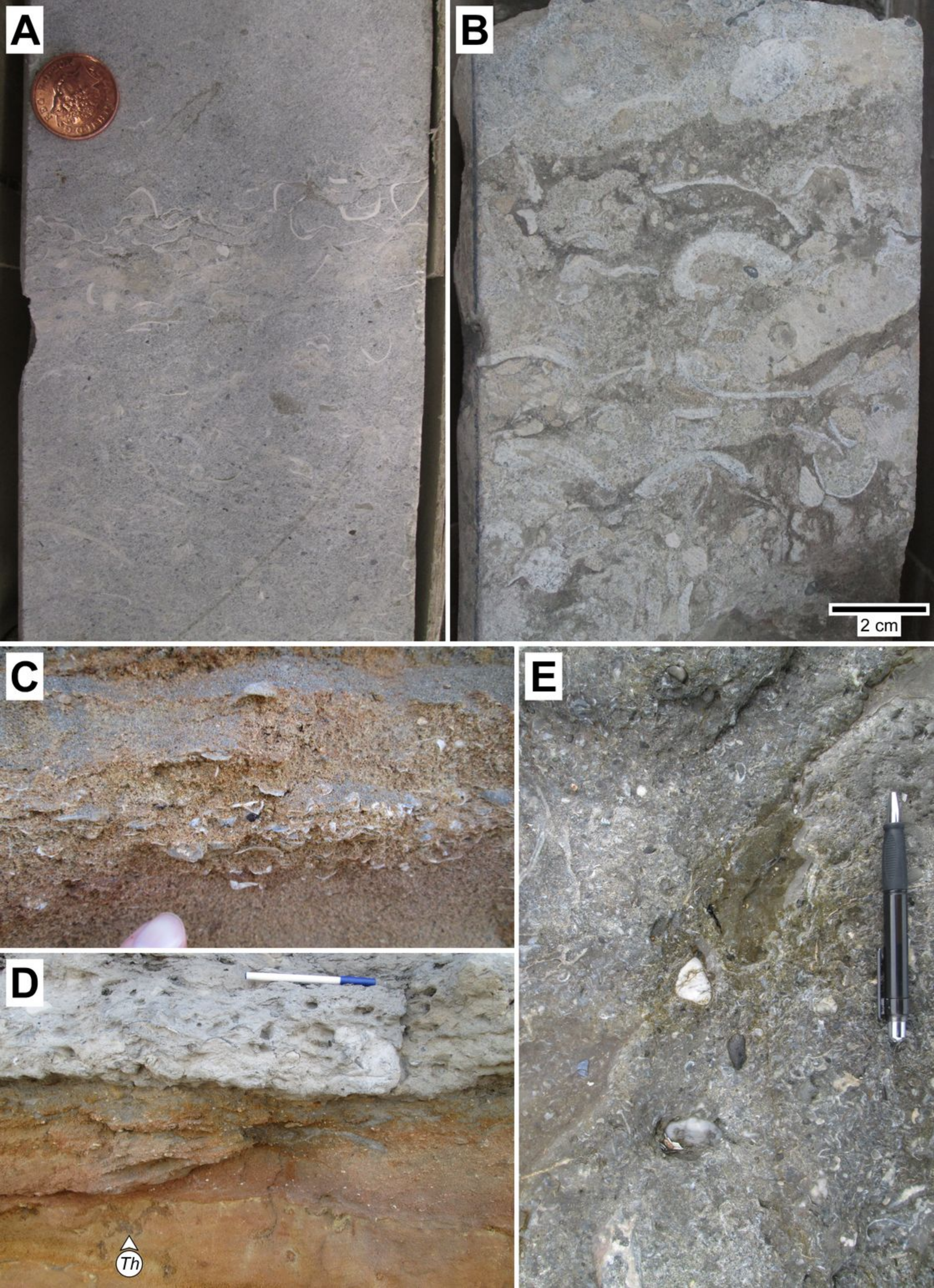
A
B
2 cm
C
E
D
Th

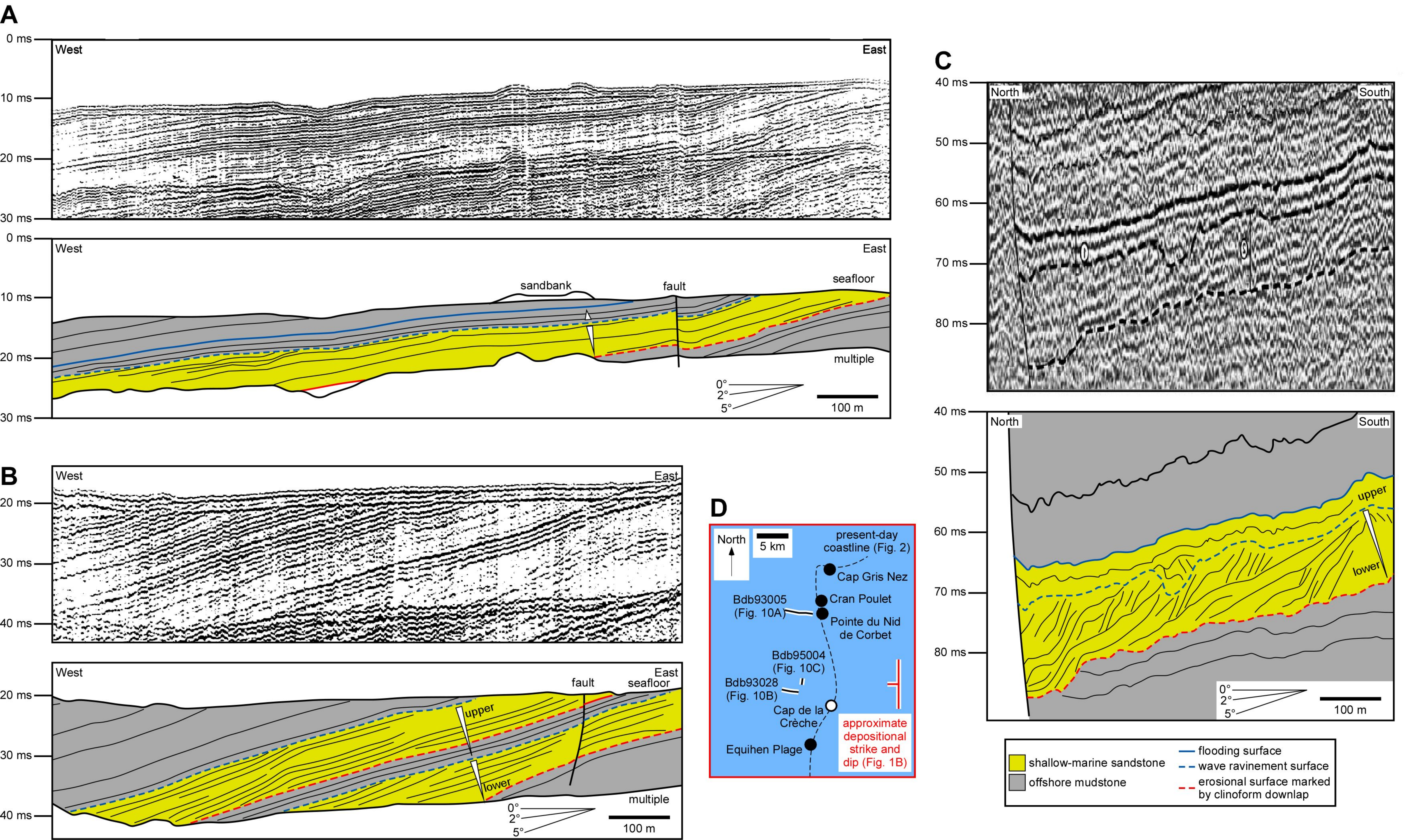

A
West
East
sandbank
fault
seafloor
multiple
100 m
0 ms
10 ms
20 ms
30 ms
0°
2°
5°
B
West
East
fault
seafloor
upper
lower
multiple
100 m
20 ms
30 ms
40 ms
C
North
South
upper
lower
40 ms
50 ms
60 ms
70 ms
80 ms
100 m
D
North
5 km
present-day coastline (Fig. 2)
Cap Gris Nez
Cran Poulet
Bdb93005 (Fig. 10A)
Pointe du Nid de Corbet
Bdb95004 (Fig. 10C)
Bdb93028 (Fig. 10B)
Cap de la Crèche
Equihen Plage
approximate depositional strike and dip (Fig. 1B)
shallow-marine sandstone
offshore mudstone
flooding surface
wave ravinement surface
erosional surface marked by clinoform downlap

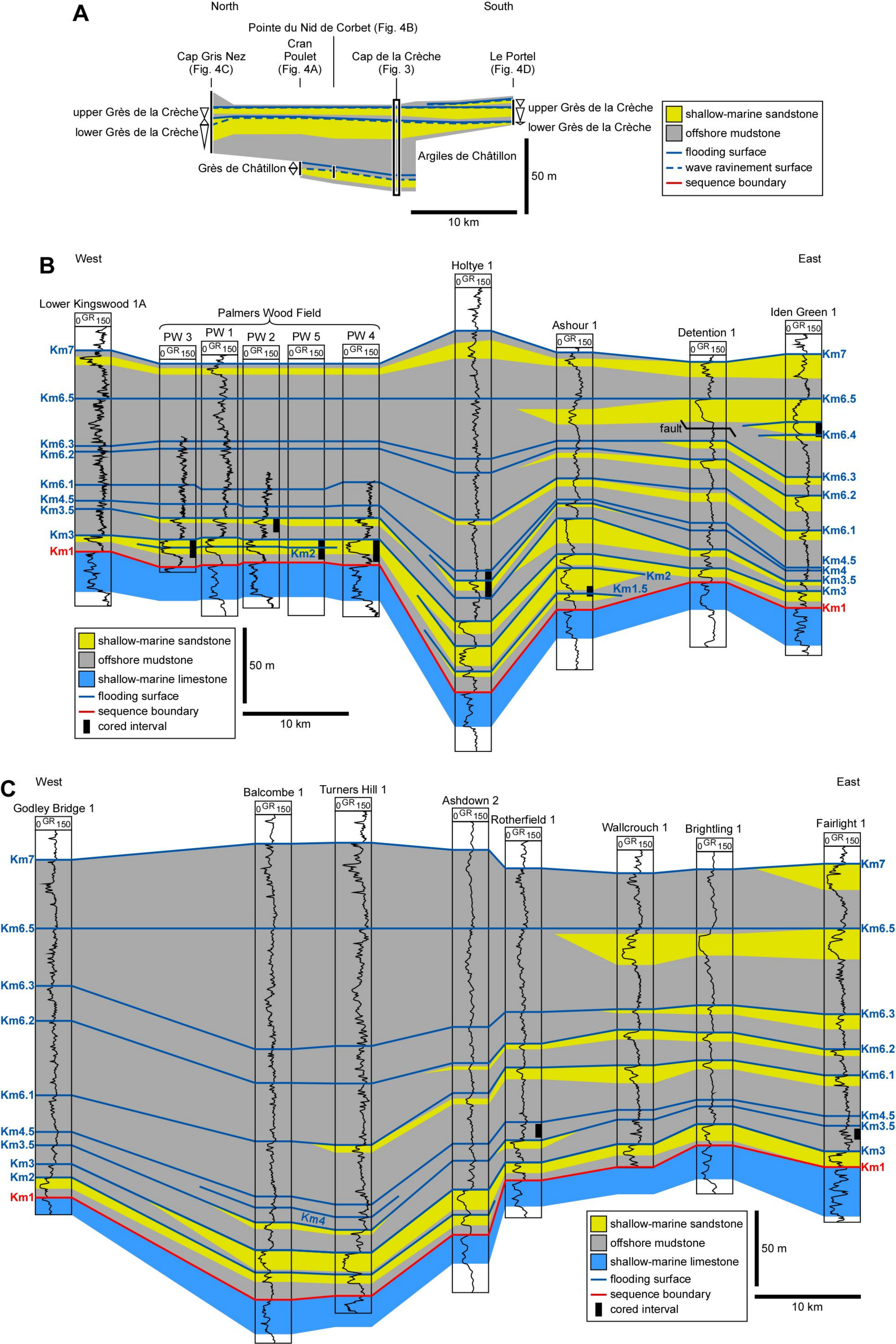

A
North
South
Pointe du Nid de Corbet (Fig. 4B)
Cap Gris Nez (Fig. 4C)
Cran Poulet (Fig. 4A)
Cap de la Crèche (Fig. 3)
Le Portel (Fig. 4D)
upper Grès de la Crèche
lower Grès de la Crèche
Grès de Châtillon
Argiles de Châtillon
50 m
10 km
shallow-marine sandstone
offshore mudstone
flooding surface
wave ravinement surface
sequence boundary
B
West
East
Lower Kingswood 1A
Palmers Wood Field
PW 3
PW 1
PW 2
PW 5
PW 4
Holtye 1
Ashour 1
Detention 1
Iden Green 1
0 GR 150
Km7
Km6.5
Km6.4
Km6.3
Km6.2
Km6.1
Km4.5
Km4
Km3.5
Km3
Km2
Km1.5
Km1
fault
shallow-marine sandstone
offshore mudstone
shallow-marine limestone
flooding surface
sequence boundary
cored interval
50 m
10 km
C
West
East
Godley Bridge 1
Balcombe 1
Turners Hill 1
Ashdown 2
Rotherfield 1
Wallcrouch 1
Brightling 1
Fairlight 1
0 GR 150
Km7
Km6.5
Km6.3
Km6.2
Km6.1
Km4.5
Km4
Km3.5
Km3
Km2
Km1
shallow-marine sandstone
offshore mudstone
shallow-marine limestone
flooding surface
sequence boundary
cored interval
50 m
10 km

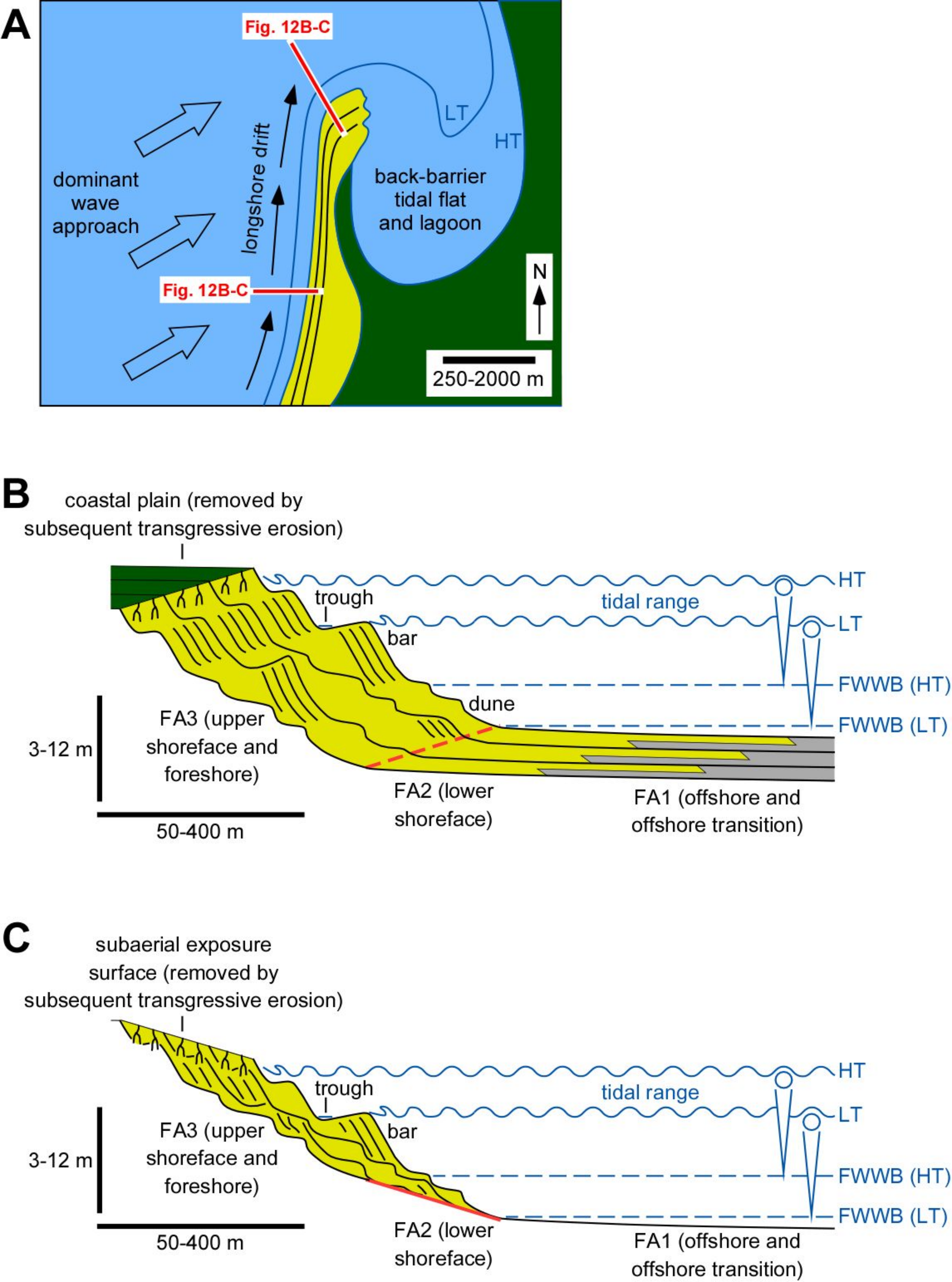
A
Fig. 12B-C
Fig. 12B-C
dominant wave approach
longshore drift
LT
HT
back-barrier tidal flat and lagoon
N
250-2000 m
B
coastal plain (removed by subsequent transgressive erosion)
trough
bar
dune
tidal range
HT
LT
FWWB (HT)
FWWB (LT)
3-12 m
FA3 (upper shoreface and foreshore)
50-400 m
FA2 (lower shoreface)
FA1 (offshore and offshore transition)
C
subaerial exposure surface (removed by subsequent transgressive erosion)
trough
bar
tidal range
HT
LT
FWWB (HT)
FWWB (LT)
3-12 m
FA3 (upper shoreface and foreshore)
50-400 m
FA2 (lower shoreface)
FA1 (offshore and offshore transition)

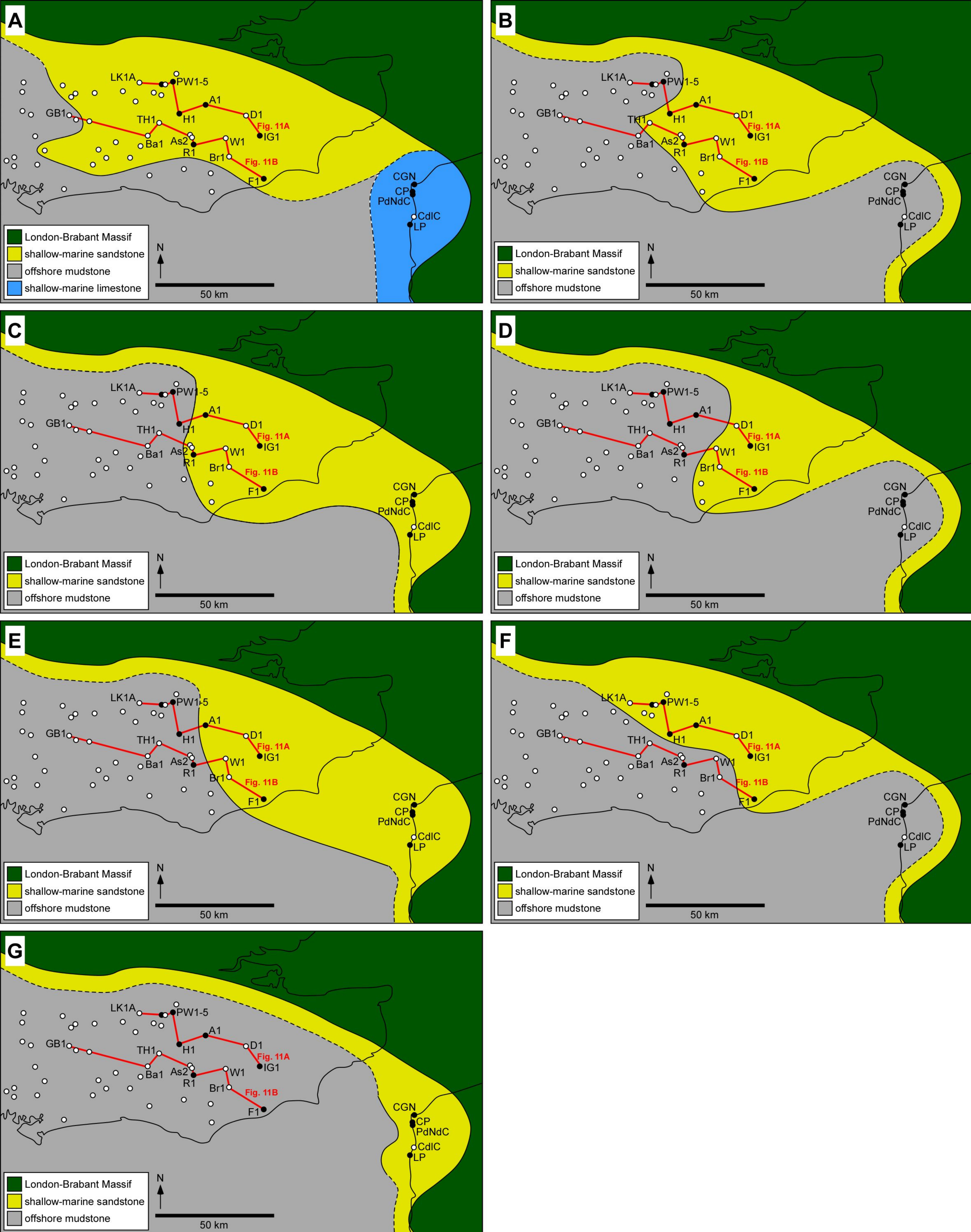

A
LK1A
PW1-5
A1
H1
D1
GB1
TH1
Fig. 11A
IG1
Ba1
As2
W1
R1
Br1
Fig. 11B
F1
CGN
CP
PdNdC
CdlC
LP
London-Brabant Massif
shallow-marine sandstone
offshore mudstone
shallow-marine limestone
N
50 km
B
LK1A
PW1-5
A1
H1
D1
GB1
TH1
Fig. 11A
IG1
Ba1
As2
W1
R1
Br1
Fig. 11B
F1
CGN
CP
PdNdC
CdlC
LP
London-Brabant Massif
shallow-marine sandstone
offshore mudstone
N
50 km
C
LK1A
PW1-5
A1
H1
D1
GB1
TH1
Fig. 11A
IG1
Ba1
As2
W1
R1
Br1
Fig. 11B
F1
CGN
CP
PdNdC
CdlC
LP
London-Brabant Massif
shallow-marine sandstone
offshore mudstone
N
50 km
D
LK1A
PW1-5
A1
H1
D1
GB1
TH1
Fig. 11A
IG1
Ba1
As2
W1
R1
Br1
Fig. 11B
F1
CGN
CP
PdNdC
CdlC
LP
London-Brabant Massif
shallow-marine sandstone
offshore mudstone
N
50 km
E
LK1A
PW1-5
A1
H1
D1
GB1
TH1
Fig. 11A
IG1
Ba1
As2
W1
R1
Br1
Fig. 11B
F1
CGN
CP
PdNdC
CdlC
LP
London-Brabant Massif
shallow-marine sandstone
offshore mudstone
N
50 km
F
LK1A
PW1-5
A1
H1
D1
GB1
TH1
Fig. 11A
IG1
Ba1
As2
W1
R1
Br1
Fig. 11B
F1
CGN
CP
PdNdC
CdlC
LP
London-Brabant Massif
shallow-marine sandstone
offshore mudstone
N
50 km
G
LK1A
PW1-5
A1
H1
D1
GB1
TH1
Fig. 11A
IG1
Ba1
As2
W1
R1
Br1
Fig. 11B
F1
CGN
CP
PdNdC
CdlC
LP
London-Brabant Massif
shallow-marine sandstone
offshore mudstone
N
50 km

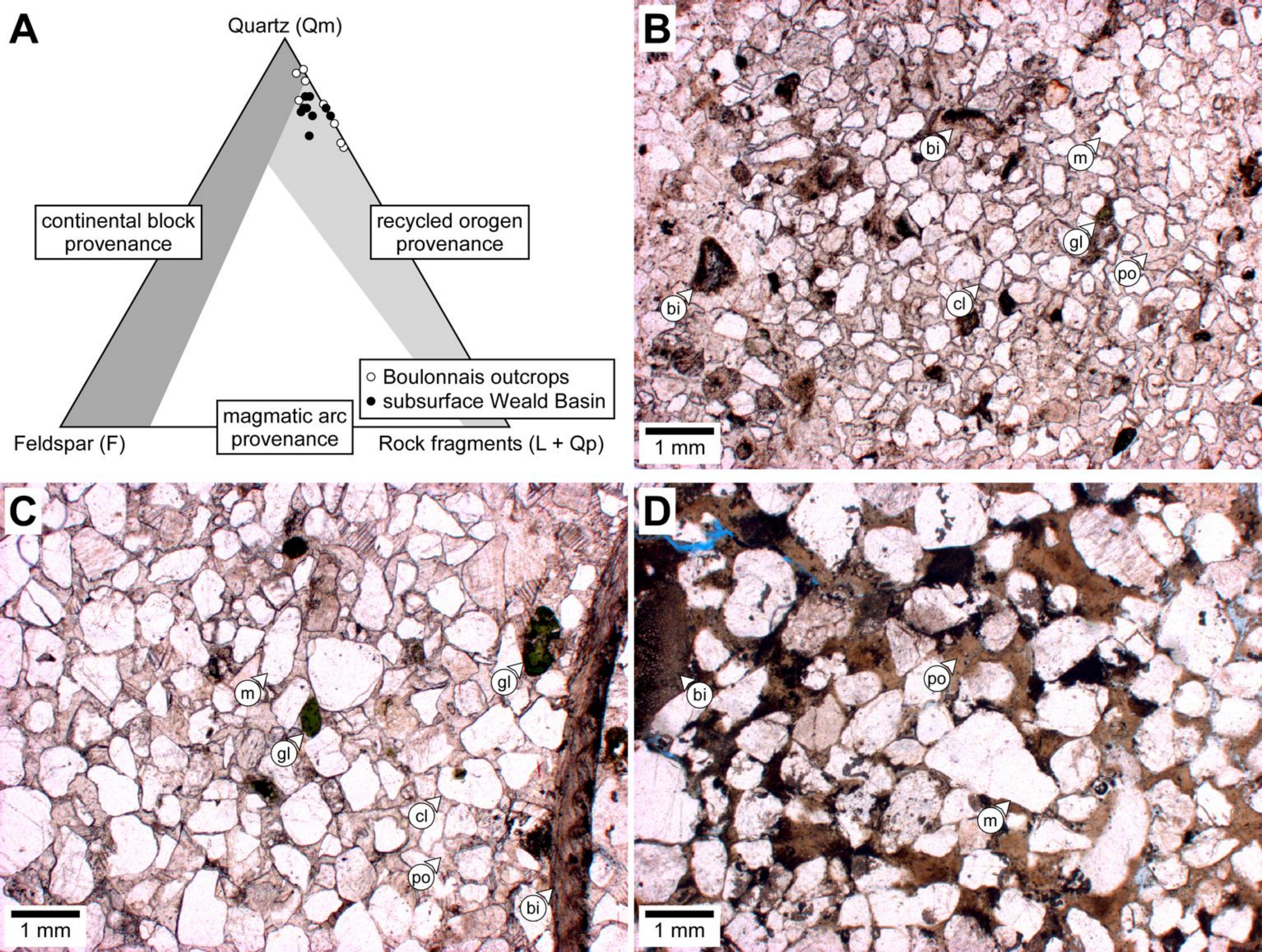

A
Quartz (Qm)
continental block provenance
recycled orogen provenance
Boulonnais outcrops
subsurface Weald Basin
magmatic arc provenance
Feldspar (F)
Rock fragments (L + Qp)
B
bi
m
gl
po
cl
bi
1 mm
C
m
gl
gl
cl
po
bi
1 mm
D
bi
po
m
1 mm

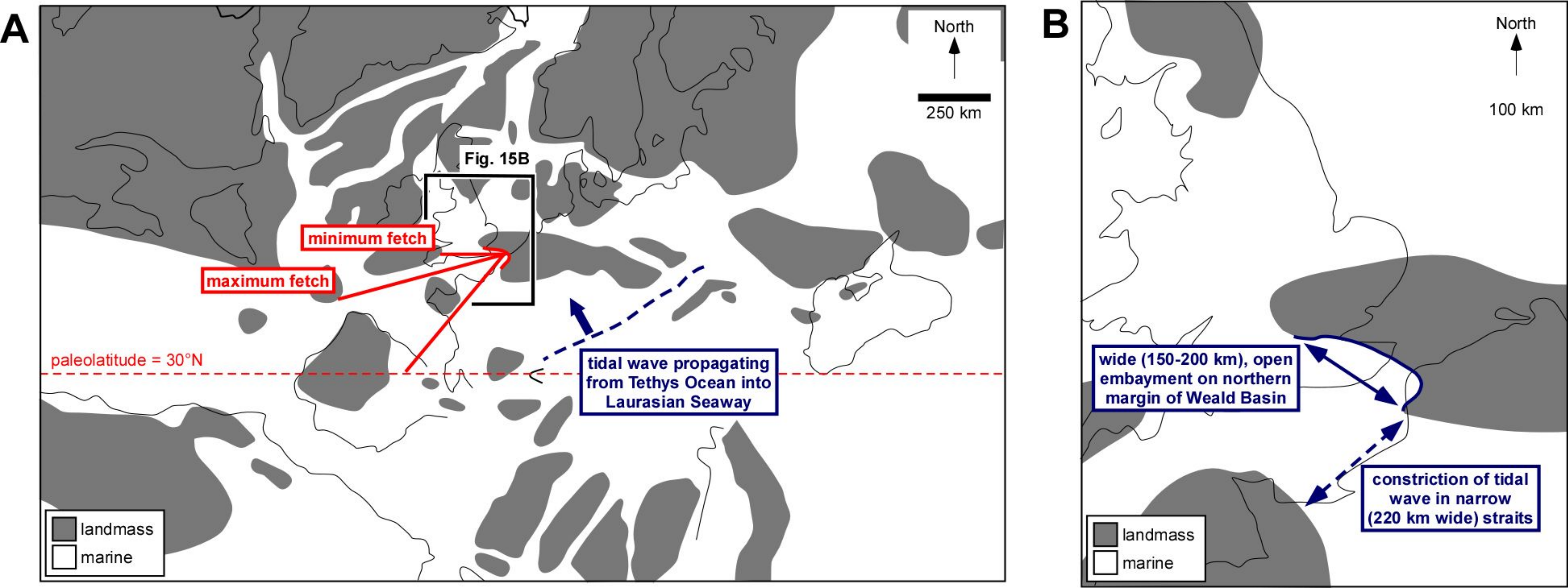
A
North
250 km
Fig. 15B
minimum fetch
maximum fetch
paleolatitude = 30°N
tidal wave propagating from Tethys Ocean into Laurasian Seaway
landmass
marine
B
North
100 km
wide (150-200 km), open embayment on northern margin of Weald Basin
constriction of tidal wave in narrow (220 km wide) straits
landmass
marine